Article:

Mulvihill, D.M., Brunskill, H., Kartal, M.E. et al. (2 more authors) (2013) A Comparison of Contact Stiffness Measurements Obtained by the Digital Image Correlation and Ultrasound Techniques. Experimental Mechanics, 53 (7). pp. 1245-1263. ISSN 0014-4851

https://doi.org/10.1007/s11340-013-9718-5

A Comparison of Contact Stiffness Measurements Obtained by the Digital Image Correlation and Ultrasound Techniques

D.M. Mulvihill[a,*], H. Brunskill[b], M.E. Kartal[a], R.S. Dwyer-Joyce[b], and D. Nowell[a]

[a] Department of Engineering Science, University of Oxford, Parks Road, Oxford OX1 3PJ, UK

[b] Department of Mechanical Engineering, University of Sheffield, Mappin Street, Sheffield S1 3JD, UK

Abstract:

The digital image correlation (DIC) and ultrasound techniques have both previously been employed to measure the contact stiffness of real engineering interfaces, but a comprehensive comparison of these techniques has not previously been carried out. Such a comparison is addressed in the present paper by a series of tests where both DIC and ultrasound are used to simultaneously measure contact stiffness in the same tests. The two techniques gave similar magnitudes for stiffness, with ultrasound being around three times stiffer at an average normal pressure of 70 MPa. Given that the techniques are vastly different in their measurement approach (DIC measures on the micron scale while ultrasound measures on the Ångstrom scale), this level of agreement is thought to be encouraging. The difference in results can partly be explained by consideration of physical differences between the techniques. Ultrasound measurement will give a local elastic 'unloading stiffness' whereas a load-deflection technique like DIC, will give a plastic 'loading stiffness'. This difference is clearly brought out in the experiments carried out under increasing tangential load. Under normal loading, the increase in real contact area obscures the effect to some extent as both DIC and ultrasound stiffnesses increase with normal load. The results suggest that rough interfaces may be satisfactorily modelled as a variable stiffness spring whose stiffness increases with contact pressure as the smooth contact case is approached.

Keywords: Contact stiffness, Digital image correlation, ultrasound, titanium alloy

* Corresponding author. Tel.: +44 1865 2 73184; *E-mail address:* dm.mulvihill@yahoo.ie (D.M. Mulvihill).

Nomenclature

c	wave speed
f	coefficient of friction
f_u	ultrasound frequency
P	total normal force
p_m	mean normal pressure
Q	total tangential force
R	reflection coefficient
S_q	areal root mean square roughness (standard deviation of surface heights)
x, y, z	Cartesian coordinates, (z is normal to a surface)
Z	acoustic impedance
Z_1, Z_2	acoustic impedance in bodies 1 and 2
κ	contact stiffness per unit nominal area
κ_n	normal (longitudinal) contact stiffness per unit nominal area
κ_t	tangential (shear) contact stiffness per unit nominal area
κ_{DIC}	contact stiffness (per unit area) measured by digital image correlation
κ_{FE}	contact stiffness derived from a finite element model
$\kappa_{Interface}$	contact stiffness of an interface isolated from other contributions
ρ	density
ω	angular frequency

Abbreviations

DIC	digital image correlation
FE	finite element
FFT	fast Fourier transform
RMS	root mean square
UPR	ultrasound pulser-receiver

1. Introduction

Contact stiffness can be defined as the change in normal or tangential load at a contact for a unit change in relative normal or tangential displacement of the surfaces in contact. Defined in this way, contact stiffness depends on the position of the reference points for displacement. For a smooth contact model, the stiffness becomes infinite as these points approach the interface. However, real contacts are microscopically rough and this leads to a finite interfacial stiffness. The contact stiffness can either be defined as an instantaneous tangent stiffness at a particular load value or as a secant stiffness taken over range of load. Contact stiffness is a particularly important parameter in the analysis of jointed structures. The vibration response (resonant frequencies etc.) of single components can be predicted extremely accurately, but when frictional joints are present, current predictive models are often unsatisfactory due to a lack of understanding of joint parameters such as contact stiffness and friction [1]. Some of the friction issues have been addressed elsewhere (e.g.[2, 3]) and here we intend to focus solely on the stiffness aspects. These are particularly important in, for example, the aerospace industry where there are a number of frictional joints which have a direct bearing on vibration response (e.g. blade-disc dovetail joints, blade underplatform dampers, and blade-tip shrouds etc. in the aeroengine, as well as bolted or riveted joints in the aircraft structure). In order to further improve physical understanding of contact stiffness, techniques for its experimental measurement must be well developed and understood. Two methods which have been applied to real engineering interfaces are the digital image correlation [4-6] and ultrasound techniques [7-17].

Ultrasound is a vibration whose frequency is above the audible range. In a 1971 study, attempting to use ultrasound to measure the real area of contact at an interface, Kendall and Tabor [7] realised that the amount of ultrasound reflected from a rough interface was directly related to the stiffness of the interface. Since a given contact stiffness can be achieved with a single large area of contact, or with a smaller area divided into a number of contact regions which are spaced apart, they concluded that the technique could not hope to directly determine the real area of contact. However, the ability to measure contact stiffness was a promising development and Tattersall [18] went on to further define and generalise how this might be done. Essentially, these two early works proposed that the interface be considered as a region having the stiffness of a simple Hookean spring (see Figure 1).

When an incident ultrasound wave passes to a region of different material stiffness (or density) through a perfect (smooth) interface, some of the wave is transmitted through, while the remainder is reflected. The proportion of the incident wave which is reflected (called the reflection coefficient) is directly related to the stiffness and density of each material. Similarly, when an ultrasonic wave is projected through a rough interface, the contact stiffness, as well as the stiffness and mass properties of the two materials, will determine the reflection coefficient. Tattersall [18] used the 'spring model' to develop a simple formula expressing the reflection coefficient R in terms of the acoustic impedance of the two materials in contact Z_1 and Z_2 (defined as the product of density and wave speed) and the interface stiffness per unit area κ.

$$R = \frac{Z_1 - Z_2 + i\omega(Z_1 Z_2/\kappa)}{Z_1 + Z_2 + i\omega(Z_1 Z_2/\kappa)}. \tag{1}$$

where ω is the angular frequency of the ultrasound. Note that wave speed (accounted for in the acoustic impedance term) is determined itself by the stiffness and density properties of a material. If, as in the case of the present work, the material on both sides of the interface is the same, then Equation (1) reduces to:

$$R = \frac{1}{\sqrt{1 + \left(\frac{2\kappa}{\omega Z}\right)^2}}. \tag{2}$$

Solving explicitly for contact stiffness gives:

$$\kappa = \frac{\omega Z}{2}\sqrt{\frac{1}{R^2} - 1}, \tag{3}$$

and substituting $\omega = 2\pi f_u$ and $Z = \rho c$ gives:

$$\kappa = \rho c f_{\mathrm{u}} \pi \sqrt{\frac{1}{R^2} - 1}, \tag{4}$$

where, f_{u} is the ultrasound frequency, ρ is the material density, and c is the wave speed in the material. Equation (4) can be used for the calculation of both normal stiffness per unit area κ_{n} and shear stiffness per unit area κ_{t} by simply using the appropriate transducer type and wave speed c (i.e. longitudinal or shear). Therefore, from experiments in which the incident wave and the reflected wave from a rough surface are recorded, the reflection coefficient R can be found, and Equation (4) used to determine the contact stiffness.

The interface model described above is quasi-static and ignores any influence of mass. Drinkwater *et al.* [12], used broadband transducers to examine frequency dependence in a single test by calculating reflection coefficients and stiffness across the frequency range of the transducer. They found that the reflection coefficient depended on frequency in the same way as predicted by the 'spring model', but showed that contact stiffness was independent of the frequency – thereby verifying the quasi-static 'spring model'. There are, however, some limitations on the frequency range which will give acceptable results. A succinct discussion of this is given in Drinkwater *et al.* [12]. If the wavelength of the ultrasound is similar to the size of the interface gaps, then complex scattering will occur where resonances are established between gaps (Rose [19]). If the wavelength is considerably smaller than the gap sizes, the results will not be affected by the gaps; however, the frequencies required to achieve this are of the order of GHz for most commonly occurring machined finishes on metals. At frequencies this high, the attenuation of the signal is too great to measure meaningful results. If wavelengths significantly greater than the gap sizes are used, however, then the reflection and transmission of ultrasound will be unaffected by the size, shape and distribution of gaps, and attenuation of the signal will be low. Therefore measurements are generally taken in the low frequency/long wavelength regime. Most work has been done on metals and the frequency range of the transducers is usually 1–20 MHz [11-17].

The ultrasound method has more often been used for the calculation of normal contact stiffness, but the approach is equally applicable to tangential stiffness as long as an appropriate ultrasonic shear transducer is used and the wave speed in shear is used in calculating acoustic impedances. The response of a rough contact to shear waves was investigated successfully by Królikowski and Szczepek [11], Baltazar *et al.* [14], Dwyer-Joyce and Gonzalez-Valadez [16], and Gonzalez-Valadez *et al.* [17]. One of the major advantages of the ultrasound technique (which was referred to in the original paper by Kendall and Tabor [7]) is that it can be applied to such a wide range of materials (i.e. metals and non-metals, transparent materials and opaque materials).

The digital image correlation technique has only recently been used to measure contact stiffness. Kartal *et al.* [4] appear to have been the first to use the technique, but further work by Kartal *et al.* [5] and de Crevoisier *et al.* [6] has followed. The DIC technique involves obtaining high resolution digital images giving side-on views of the interface (and the surrounding area) while the applied load is varied. By comparing subsequent images to one taken at the beginning of loading, displacements can be calculated on each side of the interface and then subtracted to give local relative displacement. Applied load is easily measured by a load cell; a plot of load versus relative displacement is then constructed and the slope of the curve gives the contact stiffness. Each of these three papers used the DIC technique for calculation of tangential contact stiffness during fretting tests (in gross sliding with flat-and-rounded pads contacting a flat in Kartal *et al*. [4, 5], and in partial slip for a single-bolt double lap joint in de Crevoisier *et al*. [6]).

The DIC and ultrasound techniques are radically different in their approach. Although measurements of relative displacement can be taken local to the contact interface using DIC, they are still somewhat remote from the contact compared to ultrasound, which derives its measurements directly via wave reflection from the interface itself. In addition, displacements on the micron scale are usually imparted in determining the load-deflection curve for DIC, while those involved in an ultrasound excitation are of the order of Ångstroms. Further, DIC measures from a single free surface orthogonal to the interface, while ultrasound measurements are taken from an interior region of the interface.

Given the differences in the techniques, there is considerable interest in comparing measurements taken using each. Despite this, there appears to be no available literature in which contact stiffness measurements derived from load-deflection data (such as by DIC) are compared to ultrasonically obtained stiffness values in the same test. It is possible only to perform a very rudimentary comparison of the results from the two techniques by comparing work by various researchers where the materials and contact configurations vary. For example, the DIC results of Kartal *et al*. [4, 5] can be compared to the ultrasound results of Gonzalez-Valadez *et al*. [17] and Baltazar *et al*. [14]. Kartal *et al*. [4, 5] were using Ti-6Al-4V with flat-and-rounded pads in contact with a flat, Gonzalez-Valadez *et al*. [17] were using steel-on-steel with a cylindrical punch-on-flat configuration, and Baltazar *et al*. [14] were using aluminium-on-aluminium also with the cylindrical punch-on-flat arrangement. However, it is possible to compare these results at the same average contact pressure of (70 MPa). At this pressure, Kartal *et al*. [4, 5] measured normalised stiffness values in the range 8–12 kN/mm^3, Gonzalez-Valadez *et al*. [17] measured a range of 180–650 kN/mm^3, and Baltazar *et al*. [14] noted a range of 200–700 kN/mm^3.

The figures quoted above suggest that ultrasound measurements may give higher stiffness values. However, apart from the difference in material, surface roughness, and contact configuration, there are some other differences: the results quoted from Kartal *et al*. [4, 5] are averages from in excess of 5000 gross-slip fretting cycles at constant normal pressure, while Gonzalez-Valadez *et al*. [17] and Baltazar *et al*. [14] took their results in a non-fretting situation with zero bulk tangential load applied. Since ultrasonic shear waves apply an Ångstom scale tangential displacement to the interface, this means that the results in Gonzalez-Valadez *et al*. [17] and Baltazar *et al*. [14] should be equivalent to the tangent stiffness of the load-deflection curve at the very onset of bulk tangential load application; whereas, the stiffness values reported in Kartal *et al*. [4, 5] were secant stiffness measurements taken from a number of points on the load-deflection curve in a finite region after the onset of tangential load application (which would be likely to give a lower stiffness). In addition, wear debris may have reduced the contact stiffness in the experiments of Kartal *et al*. [4, 5]. Hence, there are some reasons for the differences reported, but a comprehensive study comparing the two techniques is required. Further, most of the ultrasound work has been performed where normal load is either monotonically increased or cycled with no applied tangential loading, and there appear to be no studies available which address the effect of tangential loading on ultrasonically measured contact stiffness.

A key difference between the contact stiffness results derived from tangent values of load-deflection results and those measured using ultrasound was suggested by Kim *et al.* [15]. These authors realised that an ultrasound wave actually imparts a small scale load-unload cycle upon the bulk static load. Therefore, if the load-deflection curve is elastic both methods should measure the same stiffness. However, if there is plasticity or some source of irreversibility, the ultrasound can be expected to measure the local unloading stiffness while the load-deflection technique will be measuring the tangent stiffness of the loading curve. Although Kim *et al*. [15] demonstrated the difference by comparing the contact of two elastic spheres (equivalent to the ultrasound unloading stiffness) and two elastic-plastic spheres (equivalent to the load-deflection tangent stiffness), no direct experimental evidence demonstrating the difference has so far been reported.

In the present work, the outstanding issues discussed above are addressed by a programme of tests where DIC and ultrasound are used concurrently to measure contact stiffness in unidirectional (i.e. non-fretting) ‘first load-up’ tests on Ti-6Al-4V flat-and-rounded contacts. By assessing the level of agreement in trends and magnitudes between the techniques, the experiments aim to learn more about what each technique is measuring. Both normal and tangential contact stiffness is investigated under separate application of normal and tangential loading; thereby allowing some other aspects of the physics of contact stiffness to be investigated.

2. Overview of the experimental setup

In order to compare ultrasonically measured contact stiffness with contact stiffness measured by DIC, a test was conceived whereby both measurements could be taken from the same contact and during the same test. The setup is similar to that of Kartal *et al*. [4, 5] as the same basic pad geometry and test machine were used. Figure 2 shows a schematic diagram giving details of the configuration. As in [4, 5], the pad surfaces were flat, rectangular in shape, with two parallel rounded edges and two 90 degree edges. These pads made contact with a prismatic specimen with flat sides so that a plane surface is available for the DIC. Digital images of a field of view (FOV) local to the contact interface are captured to allow contact stiffness to be measured by DIC, while an ultrasonic transducer mounted to the back face of the each of the pads allows simultaneous contact stiffness measurement of the same interface by ultrasound. Also included in the design is the facility to control the tangential load Q and the normal load P on each of the two contact interfaces.

In the tests carried out in [4, 5], the normal load P was transferred to each pad directly via its back-face. However, in this case the loading was applied to an annular region of the pad (Figure 2) by the front face of the pad-holders. This allowed a load free area at the back of the pad for the ultrasound transducers. Figure 3 shows a photograph of a specimen in contact with two pads. The specimen mounting thread, annular pad loading region, ultrasonic transducer, and lead wires can be seen. Pads and specimens were designed so that two sizes of contact area could be tested: 80 mm^2 and 50 mm^2. For the 80 mm^2 area, the contact patch was a rectangle of length 8 mm and depth 10mm while for the 50 mm^2 interface, geometric similarity was maintained and the contact rectangle was 6.32 mm by 7.90 mm. The distance between the two contacts was always 10mm.

The pads and specimens were manufactured from the aerospace titanium alloy Ti-6Al-4V. The mechanical and chemical properties of the Ti-6Al-4V used here are given in Table 1. Both pad and specimen surfaces were ground to a nominal area based root mean square

(RMS) roughness S_q of 2.3 μm. The test equipment used to provide the required constraints, to apply and measure the loads (P and Q), and to capture the digital images is shown in Figure 4. The details shown earlier in Figure 2 are housed inside a 'work-holding block' which allows the pad-holders to slide in the direction normal to the contact interface to accommodate the normal loading which is applied by the hydraulic pistons shown (the value is determined by a pressure gauge). Figure 4 also shows the hydraulic actuator and load cell used to apply and measure tangential load, respectively. The load cell was calibrated for a full-scale range of 0-15 kN with a resolution of 1N.

3. Experimental procedures for ultrasound measurements

Since the aim of the experiments is to measure both normal and tangential contact stiffness, both longitudinal and shear ultrasonic transducers were used. These transducers were commercial, broadband, piezo-ceramic transducers supplied by Tribosonics, UK and were used as both transmitter and receiver (i.e. pulse-echo mode). The centre frequency for the longitudinal and shear transducers was approximately 9.6 and 2.3 MHz, respectively (except for the shear transducers used in tests 4, 5, 6, and 10 where a 5.2 MHz approx. shear transducer was used – see Table 2 for an outline of the testing programme). The bandwidth for the longitudinal and shear transducers (measured to a 6 dB reduction in amplitude) was approximately 4–6 MHz and 2–3 MHz, respectively. Transducers for the 80 mm^2 contact area pads were 4 mm × 4 mm in size and those for the 50 mm^2 contact were 3.16 mm × 3.16 mm; scaling the transducers in this way was carried out so that the signals would encounter the same fraction of the contact width in each case. An electrical connection to the top and bottom transducer faces is required to apply a voltage signal across the transducer which is then converted to a mechanical vibration by the piezoelectric property of the transducer material. The transducers were of the 'wrap around electrode' type so that both wires could be soldered directly to the top face even though one of these connections makes electrical contact with the bottom face only. The transducers were glued to the centre of the back face of the pads (which had been smooth ground in preparation) using a cyanoacrylate based glue. Two lead wires (Filotex 50 VMTX miniature PTFE coaxial cable) were then soldered to the transducer which was then encased in epoxy to protect the connections and the transducer.

Since the setup incorporates two contacts, a shear transducer was always placed on one pad and a longitudinal on the other. Only the right-hand contact was used for DIC, however, so the appropriate type of ultrasonic transducer for the measurement being made (i.e. longitudinal or shear) was used here, while the left-hand pad contained a transducer of the other type. Two ultrasonic pulser-receivers (UPRs) were used to generate voltage pulses to actuate the transducers. Equation (4) shows that the density and wave speeds for the material are required in order to calculate contact stiffness. A density of 4420 kg/m^3 supplied by the manufacturers, TIMET [20], was used. The speed of both longitudinal and shear waves in the material were determined experimentally using the pads by sending a pulse to the surface and back (a known distance) and recording the time taken. The measured longitudinal and shear wave speeds in the material were 6148.28 m/s and 3092.8 m/s, respectively. Since the spring model (Equation 4) relates reflection coefficient to stiffness, the main experimental task is to determine the reflection coefficient when load is applied to the surface. The reflection coefficient is simply the reflected wave divided by the incident wave (when the amplitude information is expressed in the frequency domain). The incident wave data can be obtained simply by recording the reflected wave from a metal-to-air interface, since the acoustic impedance of air is very low in comparison to a metal such as Ti-6Al-4V. Hence, the reflected wave in this case is equivalent to the incident wave. This ‘reference signal’ was recorded before testing when the pads were not in contact with the specimen. Load was then applied to the interface and the reflected signal was recorded for each load increment. The incident and reflected signals (amplitude versus time) were then amplified by the UPR, digitised by a digital oscilloscope, and passed to a computer for processing. A fast Fourier transform (FFT) was subsequently implemented using LabView software to obtain the frequency spectrum (amplitude versus frequency). The programme used the average of 50 successive pulses in obtaining the frequency spectrum. At each frequency, the amplitude of the reflected wave was then divided by the amplitude of the incident wave to obtain reflection coefficients which were then used to determine contact stiffness (Equation 4). The average reflection coefficient across the bandwidth of the transducer (upper 6 dB) was then used to calculate the contact stiffness for each load increment.

4. Experimental procedures for digital image correlation measurements

In order to measure contact stiffness using digital image correlation, images of the side face of the pad and specimen which include the contact interface are required during loading. For ease of analysis, the contact interface should be either vertical or horizontal in the images so that the x and y directions correspond to the normal and tangential directions. The interface should also be roughly in the centre of the images. To obtain the digital images during the tests a PixeLINK PL-B741U CMOS 1.3 mega-pixel monochrome digital camera [21] was used. This camera has a simple USB 2.0 interface and is based on the Cypress IBIS5 CMOS global shutter progressive scan sensor with a 2/3" optical format. This gave images of the field of view (FOV) with 1280 × 1024 pixels. In order to obtain high resolution, a Questar QM1 long distance microscope [22] with a variable zoom and a working distance of 150–355 mm was used as the lens to magnify a region local to the contact. The Questar (with the camera mounted) was fixed to a precision translation stage in order to allow focusing of the FOV (Figure 4). The optics were positioned as close as possible to the pad/specimen 'side-surface' to give maximum magnification. The resulting FOV (which was positioned at the centre of the right-hand interface) was approximately 1.3 mm × 1 mm giving a pixel size of approximately 1.02 μm. Since the images contained no known macro-scale dimensions, calibration was carried out in two ways: by performing a known displacement of the specimen and dividing by the number of pixels moved, and by measuring the distance between two distinct surface micro-features using an Alicona optical profilometer and dividing by the equivalent number of pixels. Both techniques gave a very similar result.

The imaged surfaces of the pads and specimens were not specially prepared as the original grinding operation gave sufficient features for image correlation. Illumination of the FOV was provided by a fibre-optic illuminator which gave co-axial illumination. Images were recorded initially and also with each loading increment. The digital image correlation analysis of the images was then carried out using Imetrum Video Gauge software [23]. Crucially, this software allows the placing of targets on either side of the interface and can immediately output the relative displacement which occurs between a pair of targets. Figure 5 shows an image recorded from one of the tests showing all 20 targets used for analysis. The rectangular targets were 80 × 250 pixels in size while the four square targets shown were 80 × 80 pixels.

The algorithms used by the Imetrum Video Gauge software are proprietary, but in the general, DIC software works by dividing an image into sub-regions. Relative displacements are then determined by finding the best match for the reference image sub-region in the deformed image. This is usually achieved by either maximising a cross-correlation type function, or minimising a least-squares type function. The optimisation is usually performed using some variation on the Newton-Raphson technique. However, an initial guess is required for this technique; therefore, a two-step approach is usually used. Approximate displacements with only integer level pixel accuracy are determined in the first step by assuming zero displacement gradients and using a coarse searching method. In the second step, the initial guess for the displacements is input as the starting point to the Newton-Raphson method, however, since points may displace to sub-pixel locations, interpolation to produce a continuous intensity function of grey levels in the deformed image must be performed. Schemes such as bilinear interpolation or bicubic interpolation can be used here. However, a higher-order interpolation scheme (e.g. bicubic spline or biquintic spline interpolation) is recommended (Schreier *et al.* [24] and Knasss *et al.* [25]) since they provide higher registration accuracy and better convergence than simple interpolation schemes. The result should be accurate displacement and gradient predictions for the sub-region, and by analysing many sub-regions, a full-field map of displacements and strains can be computed by the method. For the present purposes a full field analysis is not required and, in the Imetrum Video Gauge software, a single average displacement value is output and assigned to the centre of each target. More detail on the use of the digital image correlation technique is given by in two recent reviews by Pan *et al*. [26] and Hild and Roux [27].

The relative displacement measurement used for the majority of the analysis which follows was derived as an average of the relative displacements associated with each of the five pairs of targets positioned closest to the interface (i.e. targets 1&2, 13&14, 15&16, 17&18 and 19&20). Five further target pairs (i.e. targets 3&4, 5&6, 7&8, 9&10, and 11&12) were also positioned on the images in order to study the relationship between contact stiffness and distance from the interface. It is difficult to obtain data from measurement points with a spacing less than about 100 μm – This is because the interface has a finite thickness, and sufficiently sized regions are required for image correlation. Plots of load (at a single contact) versus relative normal or tangential displacement were produced for each experiment and curves were fitted to the data (using Matlab) so that the tangent stiffness values could be obtained as the slope of the curves at various points during loading. A rational polynomial function (5th degree/5th degree) was found to give a satisfactory fit to the data. Stiffness values were subsequently normalised by the nominal contact area to give stiffness per unit area (i.e. the same units as the ultrasound stiffness values given by the spring model in Equation 4). The resolution of the software quoted by Imetrum is one thousandth of a pixel size. Therefore, given that the pixel size is 1.02 μm with the present setup, the quality of the results will be limited only by any noise introduced to the images themselves by small vibrations/movements during testing.

5. Experimental programme

A total of ten experiments were carried out as shown in Table 2. In contrast to the work of Kartal *et al.* [4, 5], measurements were only taken during the first monotonic application of the tangential load. This is because the ultrasound result depends on a reference signal, and any significant surface wear would invalidate the initial reference signal. Tests 1–6 had an 80 mm^2 contact area, while tests 7–10 had a contact area of 50 mm^2. In tests 1, 2, 7 and 8, the normal load was held constant to maintain a mean contact pressure p_m of 70 MPa while the tangential load was incrementally increased up to the point of slip. This allowed the tangential contact stiffness to be measured simultaneously at the right-hand contact by both ultrasound and DIC while normal stiffness was recorded by ultrasound (only) at the left-hand contact. This procedure permitted investigation into the effect of increasing tangential load on normal and tangential contact stiffness. In tests 3, 4, 5, 6, 9, and 10, no tangential load was applied and the normal load was increased, allowing comparison of measurements of normal contact stiffness by both techniques at the right-hand contact (except for tests 5 and 6 where DIC was not used); tangential contact stiffness was measured by ultrasound only at the left-hand contact. This allowed investigation of the effect of normal pressure on both contact stiffness components. Loading was increased manually (by the hydraulic actuator of the test machine in the case of tangential load and by a hydraulic pump in the case of normal loading). At each load increment a digital image and a sequence of reflected ultrasound pulses were recorded. The ultrasound pulses were recorded separately for each contact. Tests were carried out on dry, unlubricated contacts with ambient pressure and temperature conditions.

6. Results and discussion

Figure 6 shows an example of the type of displacement profile observed in the digital images along the normal to the centre of the contact patch when tangential load was applied. Some deformation occurs in the pad and specimen, but the large discontinuity in displacement at the interface is due to the compliance caused by the rough surface interaction. It can be seen that relative displacement between points closest to the interface is dominated by this interface contribution.

Figure 6 shows tangential displacement of the pad and specimen for a particular value of tangential load (corresponding to Q/fP = 0.48) in Test 1. Figure 7, however, shows the full variation of relative tangential displacement (for the measurement points closest to the interface) with applied tangential load for each of the four tests where tangential load was increased monotonically towards slip (Tests: 1, 2, 7, & 8). The average coefficient of static friction in these four tests was 0.24 – less than the values determined for Ti-6Al-4V in Kartal *et al*. [4] which reached a steady average of about 0.6 in gross-slip fretting tests. This is because a ‘run-in’ period is required before the contact reaches an approximate steady state, but in the present tests only the initial loading is considered so that the friction remains low. The data in Figure 7 show a distinct trend even though the relative displacements are very small (increasing to a maximum of between 2–3 microns near to the point of slip). It can be seen also that the force-displacement curves here are distinctly non-linear and suggest plastic deformation. Since all the results in this section correspond to initial loading of the contacts, this plastic flow is to be expected. Also shown (in red) are the rational curve fits which were used to determine tangent stiffness at each load increment.

The resulting variation in tangential contact stiffness (obtained by DIC) with tangential load for these four tests is shown in Figure 8 together with the corresponding ultrasound stiffness values derived simultaneously from the same contact. It can be seen that as tangential loading on the contact is increased, the contact stiffness as measured by DIC decreases. The ‘ultrasound stiffness’, on the other hand, does not decrease correspondingly, and instead either remains almost constant or increases somewhat.

A possible reason for this difference was first proposed by Kim *et al*. [15] as discussed earlier. They pointed out that since rough contacts quickly become elasto-plastic as loading is increased, and because ultrasound applies a local loading-unloading cycle centred on the static stress, the ‘ultrasonic interfacial stiffness’ is actually measuring the local unloading stiffness. This will be an elastic stiffness since the stress state is taken back inside the yield locus by the small scale perturbation (of the order of Ångstroms) supplied by the ultrasound. This local unloading stiffness does not ‘feel’ the plastic softening of the asperities, and therefore, even though the tangent stiffness of the loading curve decreases due to plastic yielding of asperities, the local unloading stiffness would not be expected to change as the tangential load is increased. This is explained schematically in Figure 9.

Therefore, the closest agreement between ultrasound and DIC can be expected at the onset of tangential loading ($Q = 0$) where tangent stiffness and unloading stiffness are expected to be approximately equal. The effect discussed here, though proposed by Kim *et al.* [15] in a discussion of normal contact stiffness, had not previously been observed experimentally. Previous investigations have tended to focus, not on the variation of tangential contact stiffness with tangential load, but instead on the variation with normal load where the effect could be expected to be masked by the significant increase in the real area of contact which occurs during normal loading. This would tend to cause both the ‘ultrasonic stiffness’ and the tangent stiffness of the loading curve to increase with load. In any case, to confirm the effect, an independent technique to measure the tangent stiffness of the loading curve concurrently with the ultrasound measurements is required. The use of DIC in conjunction with ultrasound in the present work has permitted this comparison to be made. A moderate increase in ultrasonically measured shear stiffness is seen to occur in Figure 9a, b, and d. This may be due to a slight increase in contact area with tangential load owning to junction growth as first observed by McFarlane and Tabor [28]. This increase in contact area is small in comparison to that which would be expected in normal loading. The evolution of the normal contact stiffness with tangential load measured by ultrasound in Tests 1, 2, 7, and 8 is given in Figure 10. This stiffness is relatively unaffected by tangential load and good repeatability can be seen across the four independent tests.

Figure 11 shows normal force versus relative normal displacement for the four tests where both DIC and ultrasound were used to measure normal stiffness (i.e. Tests: 3, 4, 9, and 10). Again, despite the small displacements involved, a definite trend is apparent in the raw data. The rational curve fits from which tangent stiffness values were obtained are also shown. Figure 11a shows that good agreement is observed when the ‘Imterum DIC results’ are compared to those from a different software package (DaVis StainMaster by LaVision [29]).

These two packages use different algorithms for the calculations of displacements and their agreement in Figure 11a increases confidence in the results.

Figure 12 compares normal contact stiffness derived from DIC analysis (slopes of the loading curves) with that derived from ultrasound for tests 4 (contact area: 80 mm^2) and 9 (contact area: 50 mm^2). As expected, both DIC and ultrasound stiffness increase in this case owing to the increase in real area of contact with normal loading. The DIC stiffness is again greater than the ultrasound stiffness but this may be due to the fact that the ultrasound technique does not 'feel' the plastic softening of the asperities as it measures local unloading stiffness rather than tangent stiffness as discussed above.

In Figure 13, ultrasonically measured tangential contact stiffness is plotted against normal contact pressure for tests 3, 4, 6, and 9. Again, as expected, the stiffness values increase with normal load and reasonable repeatability can be observed between the four tests. The stiffness values in Figure 12 and Figure 13 appear to show fairly linear variations with contact pressure unlike, for example, the results from Gonzalez-Valadez *et al*. [17] where the stiffness varies approximately as the square root of contact pressure. This may be because the material being tested here has a high yield strength (1000 MPa) and may not display any softening behaviour until pressures greater than 200 MPa are reached. This is in agreement with a recent elastic model of tangential contact stiffness ([5]), which is based on the application of Mindlin's solution [30] for tangential loading of Hertz contacts to the statistical rough surface model of Greenwood and Williamson [31] using an exponential distribution of asperity heights.

For the ultrasound measurements in both Figure 10 and Figure 13 (and for the DIC results in Figure 8), there is no discernible difference between the stiffness per unit area results from the 80 and 50 mm^2 contact areas: this suggests that the contact stiffness [load/distance] may be proportional to nominal contact area – as was the case for the fretting situation in Kartal *et al*. [5]. In Figure 14, contact stiffness measured by DIC is compared to that given by an elastic 'smooth contact' finite element (FE) model of the pad-specimen experiment. Details of this model have already been outlined in Kartal *et al*. [4] and the results shown in Figure 14 are from the FE model in [4] with 80 mm^2 contact area (without any additional layer to represent the interface compliance). It should be noted that the 'stiffness' derived from the FE model is that which is due *only* to displacement of the 'bulk' material situated between measurement points which are deliberately spaced apart by the same amount as those in the experiments. This is done so that the 'bulk' contribution to the experimentally measured contact stiffness (found from the FE model) can be compared to the experimental result and to the 'true interface contact stiffness'. In Figure 14a and Figure 14b, tangential and normal contact stiffness are plotted against distance between measurement points, respectively.

The DIC stiffness plots shown in Figure 14a are the initial tangential contact stiffness values of the pre-sliding regime (i.e. slope of the loading curve at $Q = 0$) where tangent stiffness is expected to be closest to the elastic 'unloading stiffness' (see Figure 9). The comparison of the FE model to experimental results undertaken in Kartal *et al.* [4] was to tangential contact stiffness results obtained during gross-slip fretting wear (normal pressure: 70 MPa) where the experimental result was significantly less stiff than the elastic smooth contact FE prediction. Here also, the DIC stiffness values are considerably less than the FE result for the 70 MPa contact pressure, though they are greater (by about four times) than the corresponding DIC stiffness values quoted in Kartal *et al.* [4] – the reason for this is discussed later. An 'isolated interface stiffness' can be defined by considering the experimental interface stiffness (the DIC stiffness κ_{DIC}) as the series sum of the 'bulk stiffness' (given by the FE result κ_{FE}) and the true interface stiffness $\kappa_{\mathrm{Interface}}$ (called the 'isolated interface stiffness' here):

$$\frac{1}{\kappa_{\mathrm{DIC}}} = \frac{1}{\kappa_{\mathrm{FE}}} + \frac{1}{\kappa_{\mathrm{Interface}}}. \quad (5)$$

The 'isolated interface stiffness' is also shown in Figure 14 for the DIC result at 70 MPa normal contact pressure, and this is again similar to the raw DIC result. It can therefore be assumed that at a normal pressure of 70 MPa, the interface compliance is dominant and that proportionality of stiffness [force/distance] with nominal contact area will hold in the same way as for the fretting case in Kartal *et al.* [5]. However, Figure 14a also shows a DIC result for a normal contact pressure of 200 MPa where the tangential contact stiffness is considerably closer to the predicted FE result.

In the case of normal stiffness (Figure 14b) the experimental result at p_{m} = 70 MPa is considerably less than the FE smooth contact stiffness, though again, as the normal pressure is increased from 70 to 200 MPa, the experimental stiffness approaches the FE smooth contact elastic result. As with tangential contact stiffness, both DIC and FE stiffness values increase as the interface is approached by the measurement points – though the DIC stiffness increases by much less than the FE as it becomes dominated by the interface compliance as the interface is approached (this is also clear from the displacement profile which was shown in Figure 6). In contrast, the smooth contact model assumed in the FE means that the stiffness will tend to infinity as the reference points approach the interface.

Figures 12, 13 and 14 all show that both normal and tangential contact stiffness may be considered as variable stiffness springs whose stiffness depends on the contact pressure. Figure 14 helps to shed light on an important discrepancy between different results quoted in the literature. Some authors (e.g. Johnson [32], and O'Connor and Johnson [33]) observed that the remote load-displacement response of real contacts agreed well with a smooth contact elastic analysis. Other authors, however, (e.g. Berthoud and Baumberger [34], and Shi and Polycarpou [35]) have observed that the rough interface reduced the stiffness to well below that of the elastic smooth contact predictions.

It is suggested here that it is the degree to which the contact area approximates the smooth contact case that determines whether the contact stiffness will agree with elastic predictions or be dominated by the rough interface. Essentially, as the real area of contact approaches the apparent area of contact, a response similar to the smooth contact prediction would be expected. Whether or not a contact approximates the smooth case probably depends on factors such as contact pressure, material hardness and surface roughness. The suggestion here is that at low normal pressures; high hardness; and high roughness, contact stiffness will be controlled by the multi-asperity contacts of the rough interface, but at high normal pressures; low hardness; and low surface roughness, these contacts will merge until the contact becomes closer to the smooth contact case. When a contact is dominated by a multi-contact interface, both micro-slip on the scale of the asperities (Campañá *et al*. [36]) and extra compliance introduced by voids (Sevostianov and Kachanov [37]) tend to reduce the contact stiffness to well below the smooth contact prediction (which is based purely on bulk deformation). The hypothesis just outlined is consistent with Figure 14 where it can be seen that at the lower normal pressure (70 MPa), the contact stiffness is lower and more dominated by the rough interface, whereas at the higher pressure (200 MPa), the contact stiffness appears to approach closer to the smooth contact FE result.

This analysis would also help explain the discrepancy arising from test results in the literature. If we examine the results in the literature in more detail, the discrepancy can more easily be understood. Of those authors who found agreement with the smooth contact prediction, Johnson [32] was using smooth ball bearing type surfaces while O'Connor and Johnson [33] used a very high mean contact pressure (472 MPa). Both these authors used the sphere-on-flat arrangement. On the other hand, the authors who found that the interface roughness dominated the measured contact stiffness were using very low contact pressures (Berthoud and Baumberger [34] used mean pressures up to 0.04 MPa for their flat-on-flat tests, and Shi and Polycarpou [35] used contact pressures up to 0.055 MPa for their sphere-on-flat experiments). The authors of references [32-34] measured the response to tangential loading while [35] measured the response to normal loading, and these observations, together with the results in Figure 14, suggest that the conclusions being made here apply equally to both normal and tangential contact stiffness. In summary, the effect which the rough surface interface has upon the contact stiffness probably depends mainly upon contact pressure, surface roughness and surface hardness.

Finally, some discussion of the comparison of stiffness magnitudes is warranted. First, it is useful to compare DIC results obtained here at p_m = 70 MPa with available results on the same material (Ti-6Al-4V) taken at the same normal contact pressure using similar optical techniques in the literature. These are only available for tangential contact stiffness in gross-slip fretting tests. Kartal *et al.* [4, 5] (using DIC), obtained values between 8–12 kN/mm^3 closest to the interface using contact areas of 80 and 20 mm^2, and Proprentner [38] (by tracking two laser points on either side of the interface) obtained values of 12–20 kN/mm^3 on a much smaller rig setup with a 1 mm^2 contact area. In the present work, values of 35–45 kN/mm^3 were obtained (see Table 3). There are some important differences which explain these higher values: first, the values quoted from the literature are from fretting wear tests where wear debris will serve to reduce interface stiffness, and also, the authors in [4, 5, 38] measured the initial secant stiffness at the beginning of micro-slip rather than the initial tangent stiffness at the beginning of micro-slip. Another key difference is that the stiffness results quoted in Table 3 are the initial tangent stiffness values at the very onset of the micro-slip regime during initial loading of the contacts, whereas, those by Kartal *at al.* [4, 5] and Proprentner [38] are the initial 'unloading stiffness' at the point of motion reversal during fretting. This 'unloading stiffness' is generally expected to be elastic; though, wear debris is a complicating factor.

Turning to the comparison of DIC and ultrasound stiffness magnitudes in the present work, both can be graphically compared for tangential contact stiffness in Figure 8 and for normal stiffness in Figure 12, and numerical values of measurements by the two methods are also given for tangential and normal contact stiffness respectively in Tables 3 and 4 for p_m = 70 MPa, and Q = 0 (i.e. at the onset of tangential loading in the case of tangential stiffness).

Figure 8 and Table 3 both show that the DIC tangential contact stiffness is reasonably repeatable in the four tests where it was measured. There is some degree of variability in the ultrasound measurements of tangential contact stiffness and this may possibly be explained by noting that ultrasound is very much a local measurement derived from a sub-region at the centre of the interface (which will be similar in size and shape to the emitting transducer) and will depend intimately on the contact which occurs in this region. Therefore, it can be sensitive to specimen misalignment, and small changes in local roughness and waviness etc. Since the DIC measurement is taken from points located some 50 microns or so from the interface, it is less likely to vary since it depends more on the behaviour of the whole contact region. On average (based on all data in Tables 3 and 4), the ultrasound is approximately 2.7 times stiffer than the DIC result for tangential stiffness and 3.5 times stiffer for normal contact stiffness. However, given that the two techniques are widely different in their method of measurement, the fact that the agreement in magnitude is this close is noteworthy. Particular good agreement between DIC and ultrasound can be seen graphically for normal stiffness in Figure 12. An analysis of available results in the literature was outlined in the introduction where tangential contact stiffness data from separate ultrasound and DIC studies were compared. Although those tests did not have the same materials; contact geometry; surface topography; or testing regime, their finding that the ultrasound results were stiffer is consistent with the conclusions being made here.

In attempting to understand why ultrasound gives a stiffer result, the following points should be noted. As we have seen, ultrasound gives the local unloading stiffness, whereas DIC gives the tangent stiffness. This argument can be used to explain the stiffer result for normal stiffness; however, for tangential stiffness, as long as both stiffness values are determined at the very onset of micro-slip ($Q = 0$), the effect should not be very important. In addition, the DIC result is derived from points located some 50 microns or so into the bulk, whereas the ultrasound result is derived directly from the interface itself where stiffness is expected to be higher (Figure 14 illustrates the predicted rise in stiffness as the interface is approached) – this argument applies to both normal and tangential stiffness. Also, in the case of tangential loading, it is difficult to obtain an accurate stiffness by DIC at $Q = 0$ since the relative displacement data can be difficult to interpret until Q is increased sufficiently (see Figure 6.14c).

7. Conclusions

In this work a comparison of concurrent DIC and ultrasound measurements was undertaken in a series of unidirectional 'first load-up tests' where either the normal or tangential load was incrementally increased. Despite the small displacements involved (< 2–3 μm up to slip in the case of tangential loading), the DIC technique was seen to produce distinct load versus relative displacement curves for both normal and tangential loading cases. The load-displacement curves were non-linear indicating plastic flow: as would be expected from initial loading of a rough contact. For the first time, a fundamental difference (proposed by [15]) between the tangent stiffness taken from the loading curve and the 'ultrasonic stiffness' was observed: ultrasound always measures the local unloading stiffness which is elastic and unaffected by the plastic softening of asperities tending to reduce the tangent stiffness. This effect was observed experimentally in the present work in the tangential loading case where DIC stiffness was seen to reduce towards zero as loading proceeded; whereas, the ultrasound saw no reduction in tangential contact stiffness. For normal contact stiffness, both DIC and ultrasound values increased with normal load due to the increase in real area of contact which masks this effect (though normal stiffness measured by DIC was less stiff than ultrasound at equivalent normal loads – probably owing to plastic softening lowering the DIC stiffness but not the ultrasound stiffness). In agreement with the work of previous researchers, tangential and normal contact stiffness were both found to increase with normal loading.

When compared to the DIC results derived by [4] during gross-slip fretting tests, the tangential contact stiffness values obtained here by DIC in the unidirectional tests were about four times stiffer – this may be due, among other things, to the tendency of wear debris in the fretting tests to reduce contact stiffness. The DIC results for contact stiffness arising from these unidirectional tests were also compared to stiffness values derived from a smooth contact FE model. For the lower contact pressure (70 MPa), the contact stiffness was dominated by the compliance of the rough interface. However, when the contact pressure was increased to 200 MPa, the contact stiffness approached closer to the smooth contact elastic FE result. This suggests that at low pressures the multi-asperity contacts dominate the contact stiffness, but as the pressure is increased, these contacts merge to form a contact which begins to more closely approximate the smooth contact case. Therefore, at lower normal contact pressures, the result that contact stiffness is proportional to nominal contact area can be true even for the non-fretting case; in fact, the results show that no discernible difference in ultrasound and DIC contact stiffness (per unit area) between the 80 and 50 mm^2

contacts can be observed at 70 MPa. It was hypothesised (based on results here and in the literature) that the degree to which contact stiffness depends upon bulk deformation (when measured remotely) depends on how well the contact approximates the smooth contact equivalent. Following from this analysis, it seems reasonable to suggest that the extent to which the contact stiffness depends upon the interface will depend on three main factors: contact pressure, surface roughness, and surface hardness.

Turing finally to comparison of magnitudes, given the vast difference between the two methods, the fact that corresponding stiffness values are of the same order of magnitude is firstly of interest. Ultrasound was always stiffer than DIC: on average, for normal stiffness, the ultrasound result at p_{m} = 70 MPa was about 3.5 times stiffer than DIC, and for tangential stiffness, the ultrasound result at p_{m} = 70 MPa was 2.7 times stiffer. This disagreement is sufficiently small so that a question cannot be raised about the validity of either method especially given that ultrasound measures local unloading stiffness whereas DIC measures tangent stiffness. However, it does seem that there is quite a degree of variability in the ultrasound measurements which are probably more sensitive to local contact and roughness conditions than DIC. DIC may be more robust in certain circumstances since its measurement depends more on the entire contact (as the measurement points are somewhat removed from the surface). There are disadvantages to the DIC technique also, such as the fact that a reliable tangential contact stiffness measurement at the very onset of micro-slip is difficult to determine due to the small displacements and the 'slack' involved before the load is sufficiently increased. Choosing which technique to use in a given case will depend on which technique can be physically accommodated. Also if tangent stiffness is required, DIC is the obvious choice, whereas ultrasound is suited to measuring the elastic local unloading stiffness. In addition, DIC is more suited to measuring contact stiffness in fretting tests as the ultrasound reference signal is invalidated by surface wear in fretting.

To improve comparison between ultrasound and digital image correlation measurements of contact stiffness, more focus should be given to making the comparison during unloading rather than loading since the quantity being measured by each technique should be more similar. A comprehensive study on how factors such as contact pressure, surface topography, surface hardness, and surface chemistry affect the extent to which remotely measured contact stiffness departs from theoretical smooth contact predictions would also be useful.

Acknowledgments

The authors would like to acknowledge the financial support of the Engineering and Physical Sciences Research Council (EPSRC) under grant reference EP/E058337/1: “A Predictive Approach to Modelling Frictional Joint Performance (PAMFJP)”. Mr Richard Duffin and Mr Wolfgang Mix and also thanked for their work on machining the various test components. Thanks are due also to the British Society for Strain Measurement (BSSM) and Imetrum Ltd for providing the digital image correlation software as part of the 2011 Young Stress Analyst Competition first prize which was awarded to the first author.

References

[1] Segalman, D. J., Bergman, L. A., and Ewins, D. J., 2007, "Report of the SNL/NSF International Workshop on Joint Mechanics", Arlington, Virginia, 16-18 October 2006, Sandia Report 2007-7761. Sandia National Labs, Albuquerque, NM.
[2] Mulvihill, D. M., Kartal, M. E., Olver, A. V., Nowell, D., and Hills, D. A., 2011, "Investigation of non-Coulomb friction behaviour in reciprocating sliding," Wear, 271(5-6), pp. 802-816.
[3] Mulvihill, D. M., Kartal, M. E., Nowell, D., and Hills, D. A., 2011, "An elastic–plastic asperity interaction model for sliding friction," Tribology International, 44(12), pp. 1679-1694.
[4] Kartal, M. E., Mulvihill, D. M., Nowell, D., and Hills, D. A., 2011, "Determination of the frictional properties of titanium and nickel alloys using the digital image correlation method," Experimental Mechanics, 51(3), pp. 359-371.
[5] Kartal, M. E., Mulvihill, D. M., Nowell, D., and Hills, D. A., 2011, "Measurements of pressure and area dependent tangential contact stiffness between rough surfaces using digital image correlation," Tribology International, 44(10), pp. 1188-1198.
[6] de Crevoisier, J., Swiergiel, N., Champaney, L., and Hild, F., 2012, "Identification of in situ frictional properties of bolted assemblies with digital image correlation," Experimental Mechanics, 52(6), pp. 561-572.
[7] Kendall, K., and Tabor, D., 1971, "An ultrasonic study of the area of contact between stationary and sliding surfaces," Proceedings of the Royal Society of London. Series A, Mathematical and Physical Sciences, 323(1554), pp. 321-340.
[8] Królikowski, J., Szczepek, J., and Witczak, Z., 1986, "High pressure in ultrasonic study of contact of solids," Physica B+C, 139-140, pp. 803-805.
[9] Królikowski, J., Szczepek, J., and Witczak, Z., 1989, "Ultrasonic investigation of contact between solids under high hydrostatic pressure," Ultrasonics, 27(1), pp. 45-49.
[10] Królikowski, J., and Szczepek, J., 1991, "Prediction of contact parameters using ultrasonic method," Wear, 148(1), pp. 181-195.
[11] Królikowski, J., and Szczepek, J., 1993, "Assessment of tangential and normal stiffness of contact between rough surfaces using ultrasonic method," Wear, 160(2), pp. 253-258.
[12] Drinkwater, B. W., Dwyer-Joyce, R. S., and Cawley, P., 1996, "A study of the interaction between ultrasound and a partially contacting solid-solid Interface," Proceedings: Mathematical, Physical and Engineering Sciences, 452(1955), pp. 2613-2628.

[13] Dwyer-Joyce, R. S., Drinkwater, B. W., and Quinn, A. M., 2001, "The use of ultrasound in the investigation of rough surface interfaces," Journal of Tribology, 123(1), pp. 8-16.
[14] Baltazar, A., Rokhlin, S. I., and Pecorari, C., 2002, "On the relationship between ultrasonic and micromechanical properties of contacting rough surfaces," Journal of the Mechanics and Physics of Solids, 50(7), pp. 1397-1416.
[15] Kim, J.-Y., Baltazar, A., and Rokhlin, S. I., 2004, "Ultrasonic assessment of rough surface contact between solids from elastoplastic loading-unloading hysteresis cycle," Journal of the Mechanics and Physics of Solids, 52(8), pp. 1911-1934.
[16] Dwyer-Joyce, R. S., and Gonzalez-Valadez, M., 2004, "Ultrasonic determination of normal and shear interface stiffness and the effect of Poisson's ratio", in Dalmaz, G., Lubrecht, A. A., Dawson, D., and Priest, M., eds., Transient processes in tribology: Proceedings of the 30th Leeds-Lyon Symposium, Lyon, France, Sept 2nd - 5th.
[17] Gonzalez-Valadez, M., Baltazar, A., and Dwyer-Joyce, R. S., 2010, "Study of interfacial stiffness ratio of a rough surface in contact using a spring model," Wear, 268(3-4), pp. 373-379.
[18] Tattersall, H. G., 1973, "The ultrasonic pulse-echo technique as applied to adhesion testing," Journal of Applied Physics D: Applied Physics, 6(7), pp. 819-832.
[19] Rose, J. H., 1989, "Ultrasonic reflectivity of diffusion bonds" in Review of progess in quantitative NDE, Thompson D.O and Chimenti D.E., eds., vol 8B, pp. 1925-1931.
[20] TiMetal 6-4 datasheet, 2000, Titanium Metals Corporation (TIMET), Hartford, CT, USA.
[21] PixeLINK PL-B741U monochrome camera data sheet, 2009, PixeLINK, Ottawa, Canada.
[22] Questar QM1 Long Distance Microscope Datasheet, Questar Corporation, New Hope, PA, USA.
[23] Video Gauge User Guide, 2009, Imetrum Limited, Bristol, UK.
[24] Schreier, H. W., Braasch, J. R., and Sutton, M. A., 2000, "Systematic errors in digital image correlation caused by intensity interpolation," Optical Engineering, 39(11), pp. 2915-2921.
[25] Knauss, W. G., Chasiotis, I., and Huang, Y., 2003, "Mechanical measurements at the micron and nanometer scales," Mechanics of Materials, 35(3-6), pp. 217-231.
[26] Pan, B., Qian, K., Xie, H., and Asundi, A., 2009, "Two-dimensional digital image correlation for in-plane displacement and strain measurment: a review," Measurement Science and Technology, 20(6), pp. 1-17.
[27] Hild, F., and Roux, S., 2006, "Digital image correlation: from displacement measurement to identification of elastic properties – a review," Strain, 42(2), pp. 69-80.
[28] McFarlane, J. S., and Tabor, D., 1950, "Relation between friction and adhesion," Proceedings of the Royal Society of London. Series A. Mathematical and Physical Sciences, 202(1069), pp. 244-253.
[29] DaVis StrainMaster 2D Software Product Manual, 2010, LaVision GmbH, Goettingen, Germany.
[30] Mindlin, R. D., 1949, "Compliance of elastic bodies in contact," Journal of Applied Mechanics., 16, p. 259.
[31] Greenwood, J. A., and Williamson, J. B. P., 1966, "Contact of nominally flat surfaces," Proceedings of the Royal Society of London. Series A, Mathematical and Physical Sciences, 295(1442), pp. 300-319.
[32] Johnson, K. L., 1955, "Surface interaction between elastically loaded bodies under tangential forces," Proceedings of the Royal Society of London. Series A, Mathematical and Physical Sciences, 230(1183), pp. 531-548.

[33] O'Connor, J. J., and Johnson, K. L., 1963, "The role of surface asperities in transmitting tangential forces between metals," Wear, 6(2), pp. 118-139.
[34] Berthoud, P., and Baumberger, T., 1998, "Shear stiffness of a solid-solid multicontact interface," Proceedings: Mathematical, Physical and Engineering Sciences, 454(1974), pp. 1615-1634.
[35] Shi, X., and Polycarpou, A. A., 2005, "Measurement and modeling of normal contact stiffness and contact damping at the meso scale," Journal of Vibration and Acoustics, 127(1), pp. 52-60.
[36] Campañá, C., Persson, B. N. J., and Müser, M. H., 2011, "Transverse and normal interfacial stiffness of solids with randomly rough surfaces," Journal of Physics: Condensed Matter, 23(8), pp. 1-9.
[37] Sevostianov, I., and Kachanov, M., 2008, "Contact of rough surfaces: A simple model for elasticity, conductivity and cross-property connections," Journal of the Mechanics and Physics of Solids, 56(4), pp. 1380-1400.
[38] Proprentner, D., 2012, PhD thesis, Imperial College London.

TABLES

Table 1: Mechanical properties and chemical composition of Ti-6Al-4V.

	Poisson's ratio	0.2% Yield stress (MPa)	Chemical composition (wt. %)						
115	0.31	1000	Al	V	N	C	O	Fe	H	Ti
			5.5-6.8	3.5-4.5	0-0.05	0-0.08	0-0.2	0-0.4	0-0.02	Bal.

Table 2: Outline of the testing programme.

Test No.	**Contact area (mm^2)**	**Loading sequence**	**Measurement technique and parameter measured**
1 & 2	80	p_m = constant = 70 MPa, Q then increased	DIC (for κ_t) + Ultrasound (for κ_t and κ_n)
3[1] & 4	80	Q = constant = 0, p_m increased to 200 MPa	DIC (for κ_n) + Ultrasound (for κ_t and κ_n)
5	80	p_m increased to 70 MPa,	Ultrasound only (for κ_t and κ_n)
6	80	p_m increased to 200 MPa	Ultrasound only (for κ_t and κ_n)
7 & 8	50	p_m = constant = 70 MPa, Q then increased	DIC (for κ_t) + Ultrasound (for κ_t and κ_n)
9 & 10	50	Q = constant = 0, p_m increased to 200 MPa	DIC (for κ_n) + Ultrasound (for κ_t and κ_n)

[1] When p_m reached 200 MPa, tangential load Q was then applied and κ_t was measured by DIC.

Table 3: Comparison of the DIC and ultrasound measurement techniques for tangential contact stiffness measured at p_m = 70 MPa and Q = 0. Distances between measurement points for calculation of DIC relative displacements were: 137, 145, 102, and 142 µm for tests 1, 2, 7, and 8 respectively.

Test No.	**Contact area (mm^2)**	**Tangential contact stiffness, κ_t (kN/mm^3)**	
		DIC	**Ultrasound**
1	80	37	68
2	80	45	47
3	80	-	105
4	80	-	147
5	80	-	98
6	80	-	81
7	50	35	224
8	50	37	101
9	50	-	114
10	50	-	42

Table 4: Comparison of the DIC and ultrasound measurement techniques for normal contact stiffness measured at p_m = 70 MPa and Q = 0. Initial distances (before loading) between measurement points for calculation of DIC relative displacements were: 126, 135, 111, and 150 µm for Tests 3, 4, 9, and 10, respectively.

Test No.	**Contact area (mm^2)**	**Normal contact stiffness, κ_n (kN/mm^3)**	
		DIC	**Ultrasound**
1	80	-	252
2	80	-	253
3	80	101	448
4	80	80	233
5	80	-	220
6	80	-	366
7	50	-	265
8	50	-	262
9	50	73	236
10	50	56	140

FIGURES

Figure 1: Schematic diagram illustrating the quasi-static spring model for ultrasound reflection from rough interfaces.

Figure 2: Schematic diagram of the specimen and pads shown with accompanying local test setup for combined DIC–ultrasound testing.

Figure 3: Photograph of a specimen in contact with two instrumented pads.

Figure 4: Photograph of the Dartec servo-hydraulic tensile testing machine showing various features of the test setup including the camera and Questar microscope used for obtaining digital images.

Figure 5: A sample digital image of the pad-specimen interface from one of the tests showing the targets (T1 – T20) used for DIC analysis with the Imetrum Video Gauge software. (image dimensions: 1 mm × 1.3 mm)

Figure 6: Absolute displacement profile of points initially lying on the central normal to the contact patch recorded in Test 1 when $Q/fP = 0.48$ as the tangential load is increased.

Figure 7: Plots of tangential force, Q, versus relative tangential displacement derived from DIC for: (a) Test 1, (b) Test 2, (c) Test 7, and (d) Test 8. Distances between the measurement points used for calculation of relative displacement were: 137 μm for (a), 145 μm for (b), 102 μm for (c), and 142 μm for (d). Rational curve fits to the data are also shown. $p_m = 70$ MPa in each case.

Figure 8: Comparison of DIC (left) with ultrasound (right) tangential contact stiffness (per unit area). Variation with tangential load for: (a) Test 1, (b) Test 2, (c) Test 7, and (d) Test 8. Distances between measurement points for calculation of relative displacement for DIC were: 137 μm for (a), 145 μm for (b), 102 μm for (c), and 142 μm for (d). $p_m = 70$MPa.

Figure 9: Schematic diagram showing the difference between tangential contact stiffness derived from DIC (the tangent stiffness) with that derived from ultrasound (the local unloading stiffness).

Figure 10: Variation of normal contact stiffness (per unit area) measured by ultrasound with tangential load in Tests 1, 2, 7, and 8. Mean normal contact pressure is 70 MPa in each test.

Figure 11: Plots of normal force, P, versus relative normal displacement derived from DIC for: (a) Test 3, (b) Test 4, (c) Test 9, and (d) Test 10. Initial distances (at $P = 0$) between measurement points for calculation of relative displacement were: 126 μm for (a), 135 μm for (b), 111 μm for (c), and 150 μm for (d). Rational polynomial curve fits to the data are also shown.

Figure 12: Comparison of DIC with ultrasound for the variation of normal contact stiffness (per unit area) with normal contact pressure: (a) Test 4, and (b) Test 9. Initial distance between measurement points for DIC (i.e. before loading) were 135 μm for (a) and 111 μm for (b).

Figure 13: Variation of tangential contact stiffness per unit area (ultrasound only) with p_m for Tests 3, 4, 6, & 9.

Figure 14: Comparison of contact stiffness (per unit area) derived from an elastic 'smooth contact' finite element model [4] with that derived from DIC: (a) tangential contact stiffness (DIC tangent stiffness at $Q = 0$ from Test 1 and Test 3), and (b) normal contact stiffness (DIC tangent stiffness form Test 3). An 'isolated interface stiffness' for the DIC results at the 70 MPa normal pressure is also given in (a) and (b). Contact area: 80 mm^2 in both cases.

Figure 1

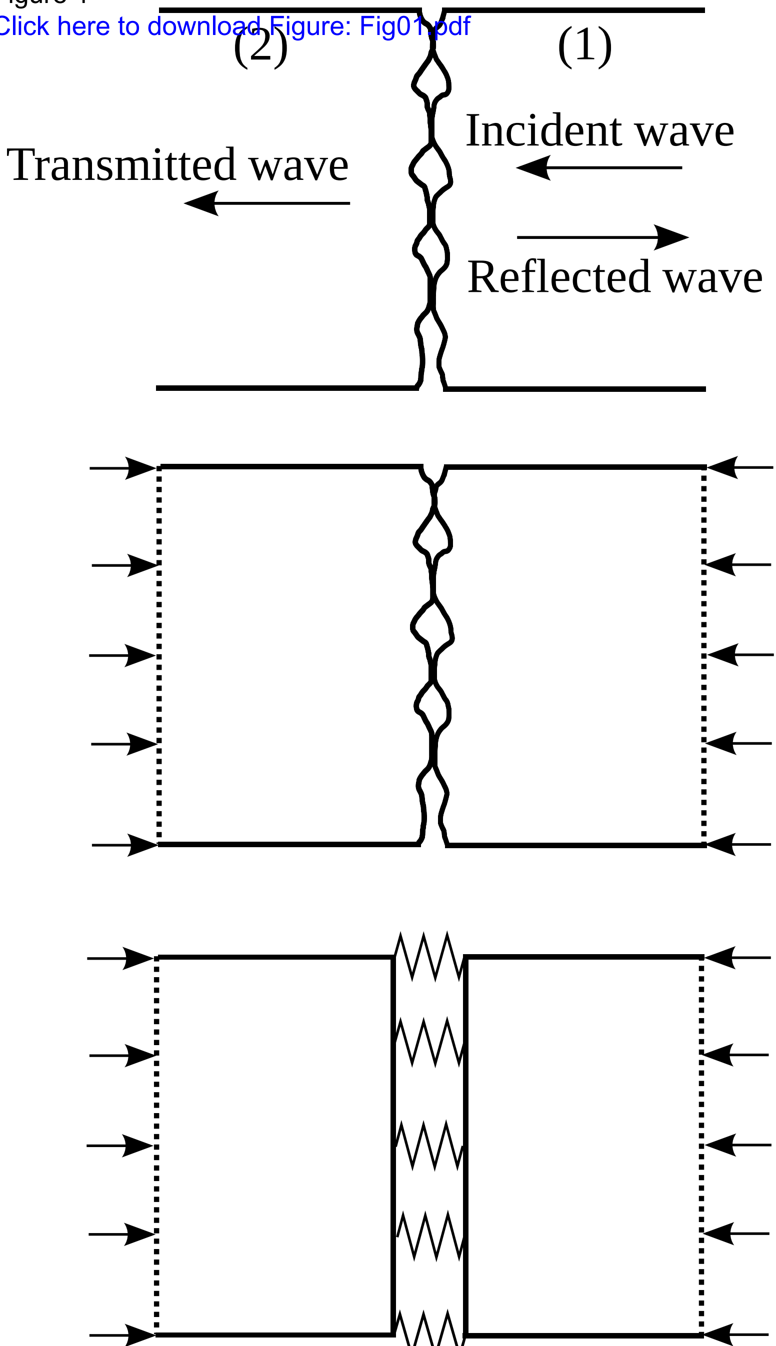

Figure 2
Click here to download Figure: Fig02.pdf

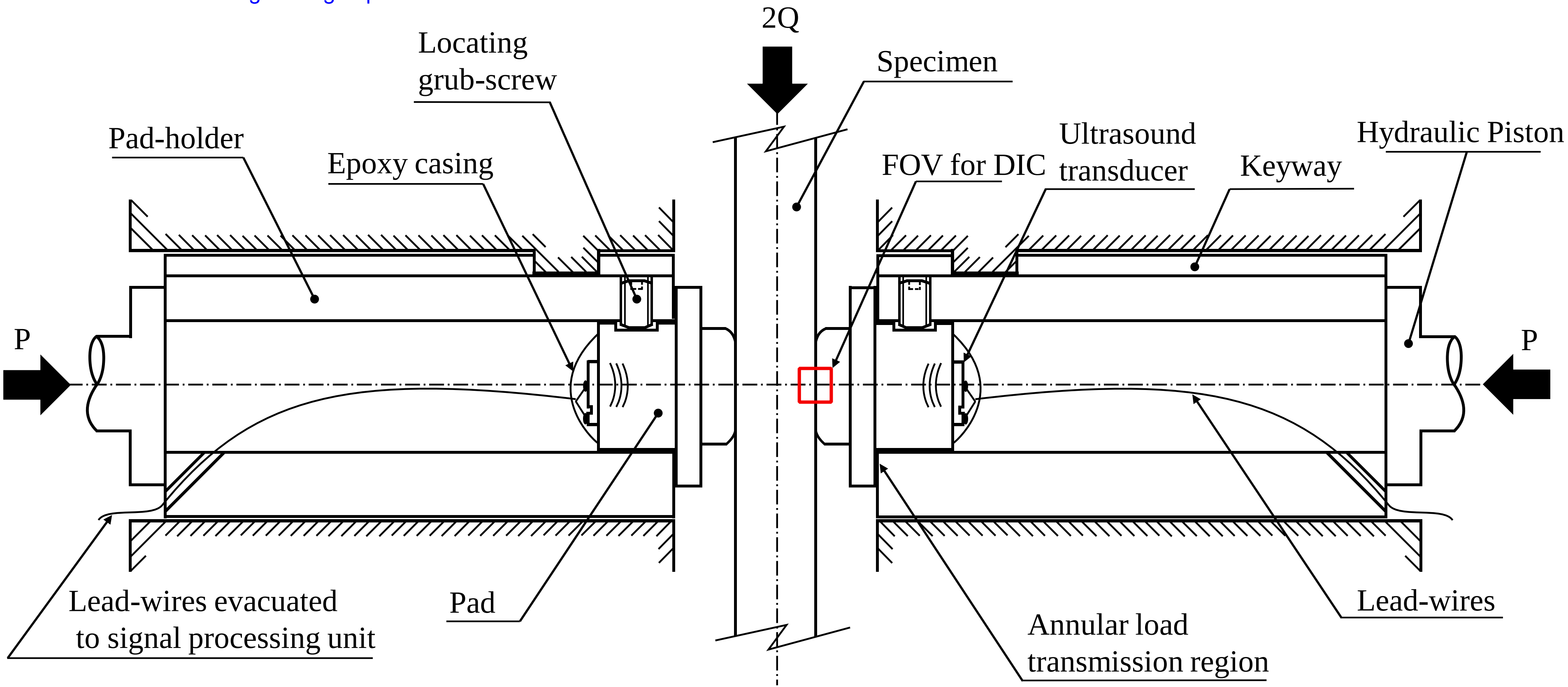

Figure 3
Click here to download high resolution image

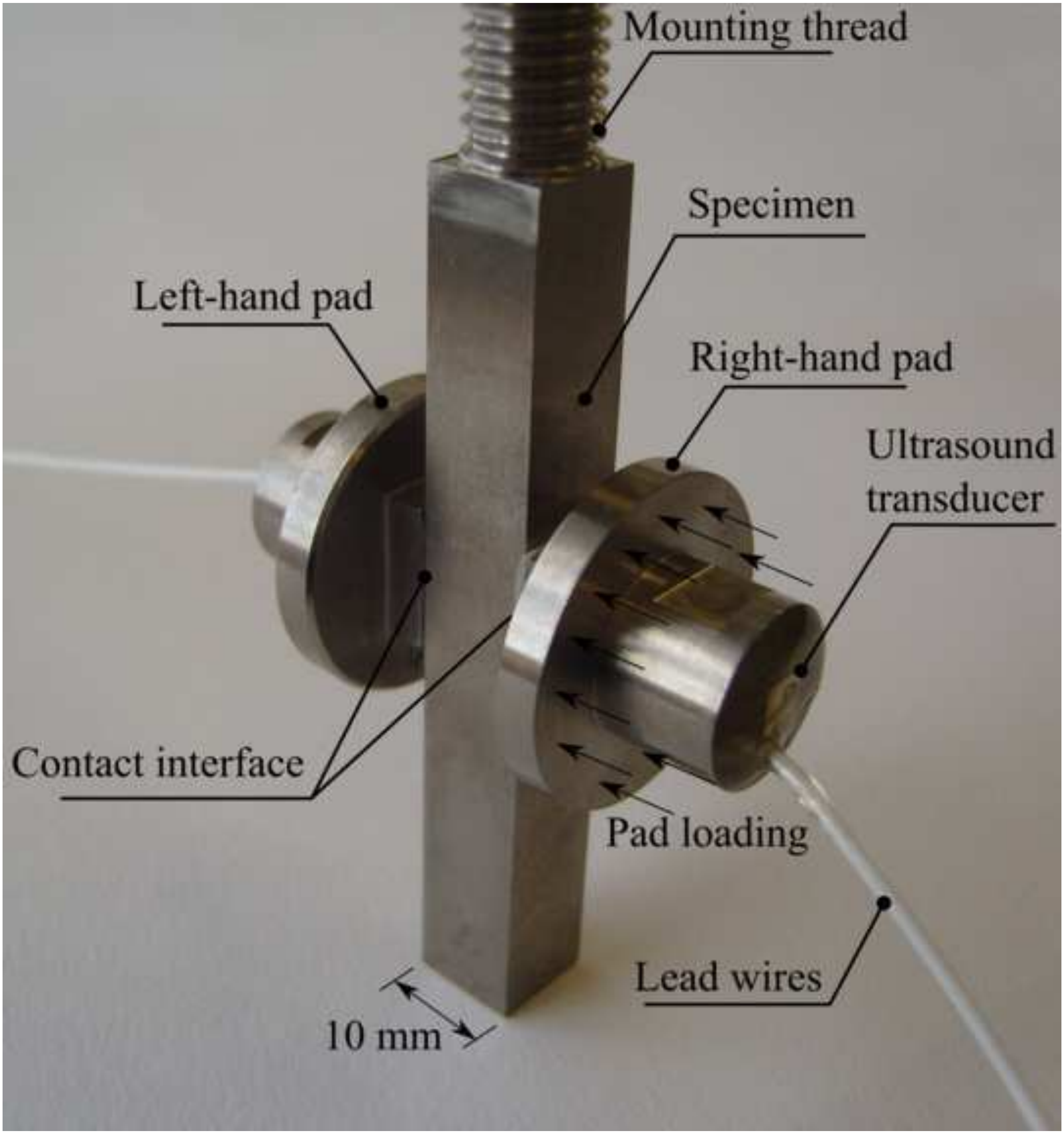

Figure 4

Click here to download high resolution image

Figure 5
Click here to download high resolution image

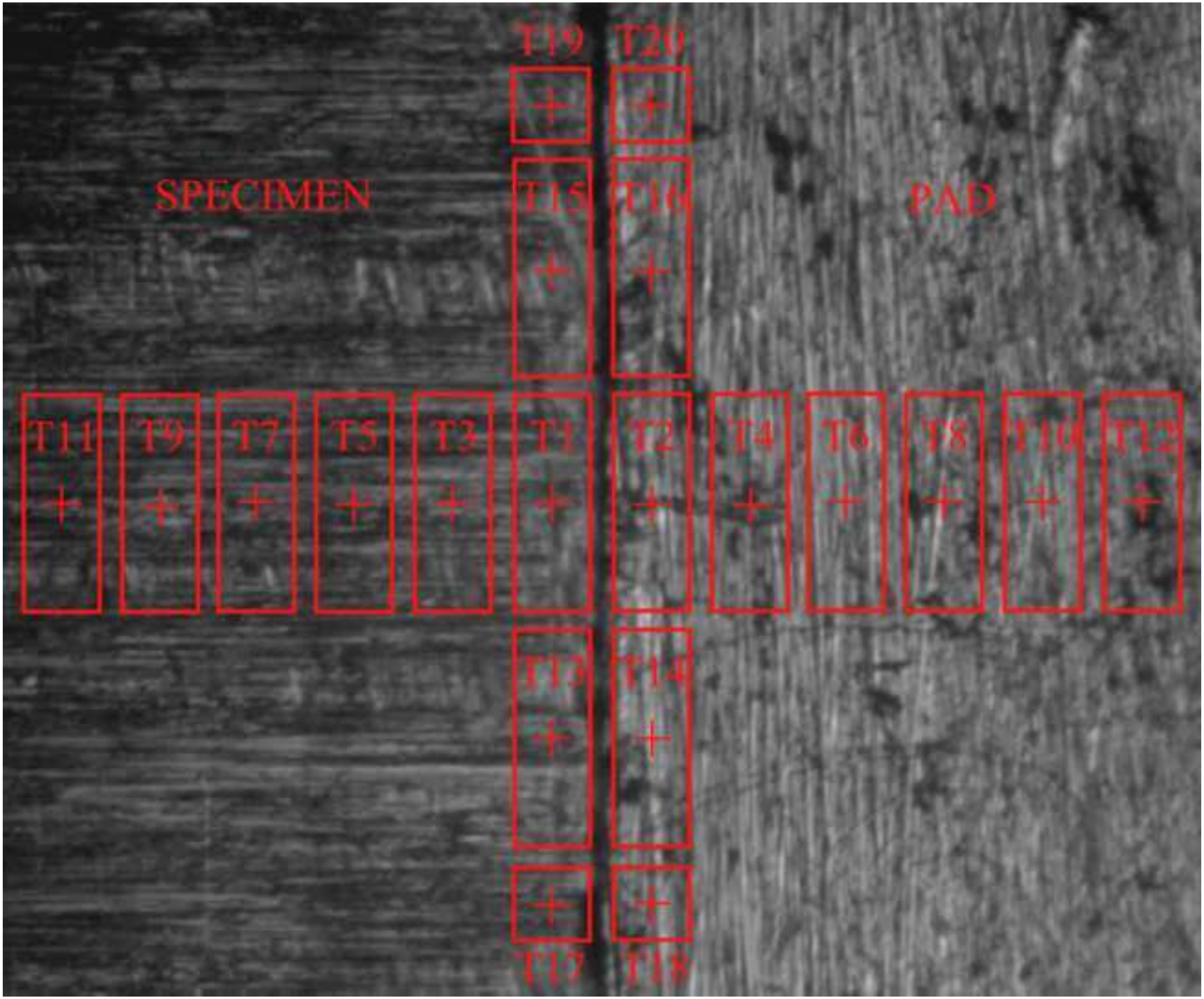

Figure 6
Click here to download Figure: Fig06.pdf

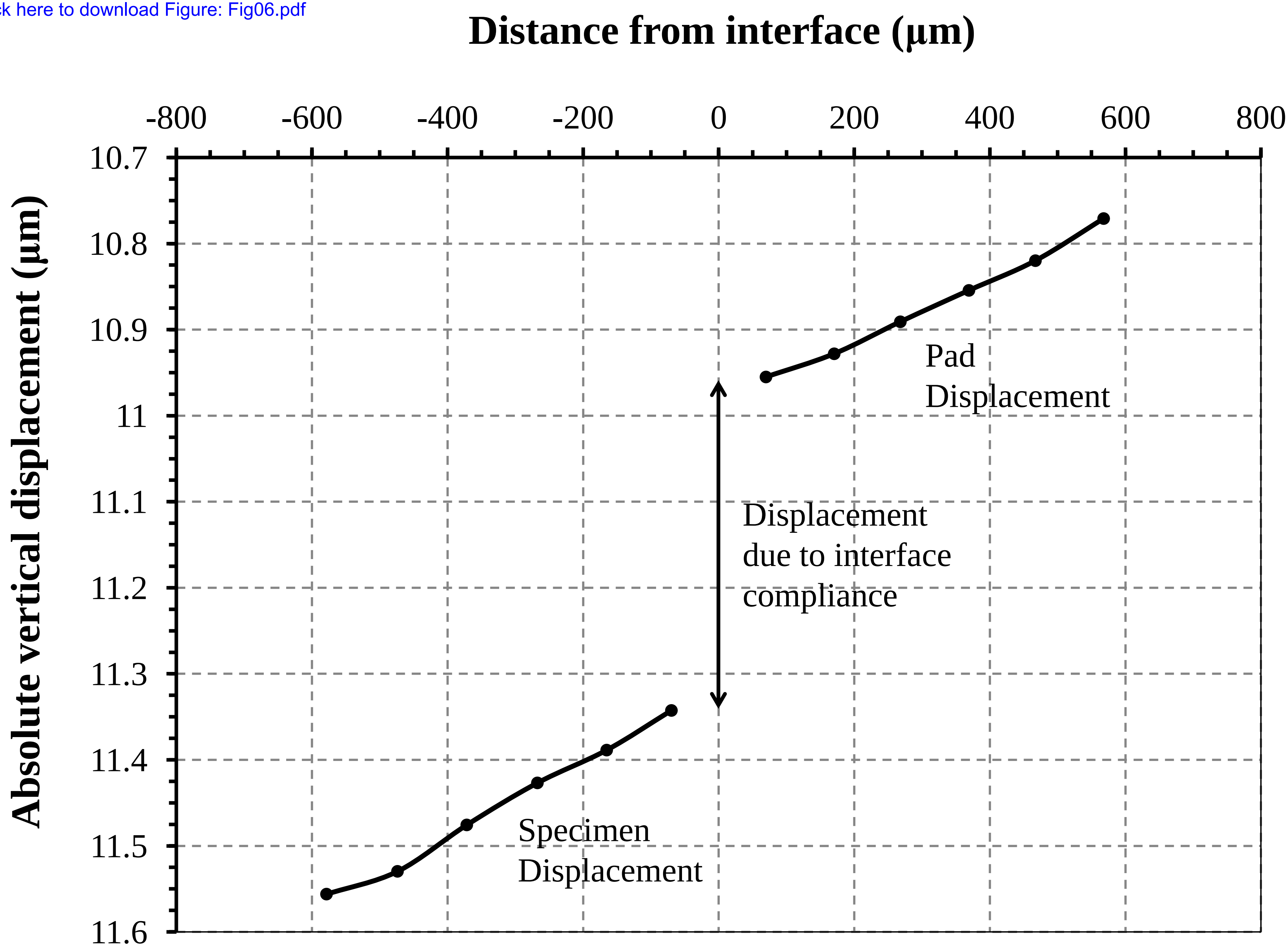

Figure 7a
Click here to download Figure: Fig07a.pdf

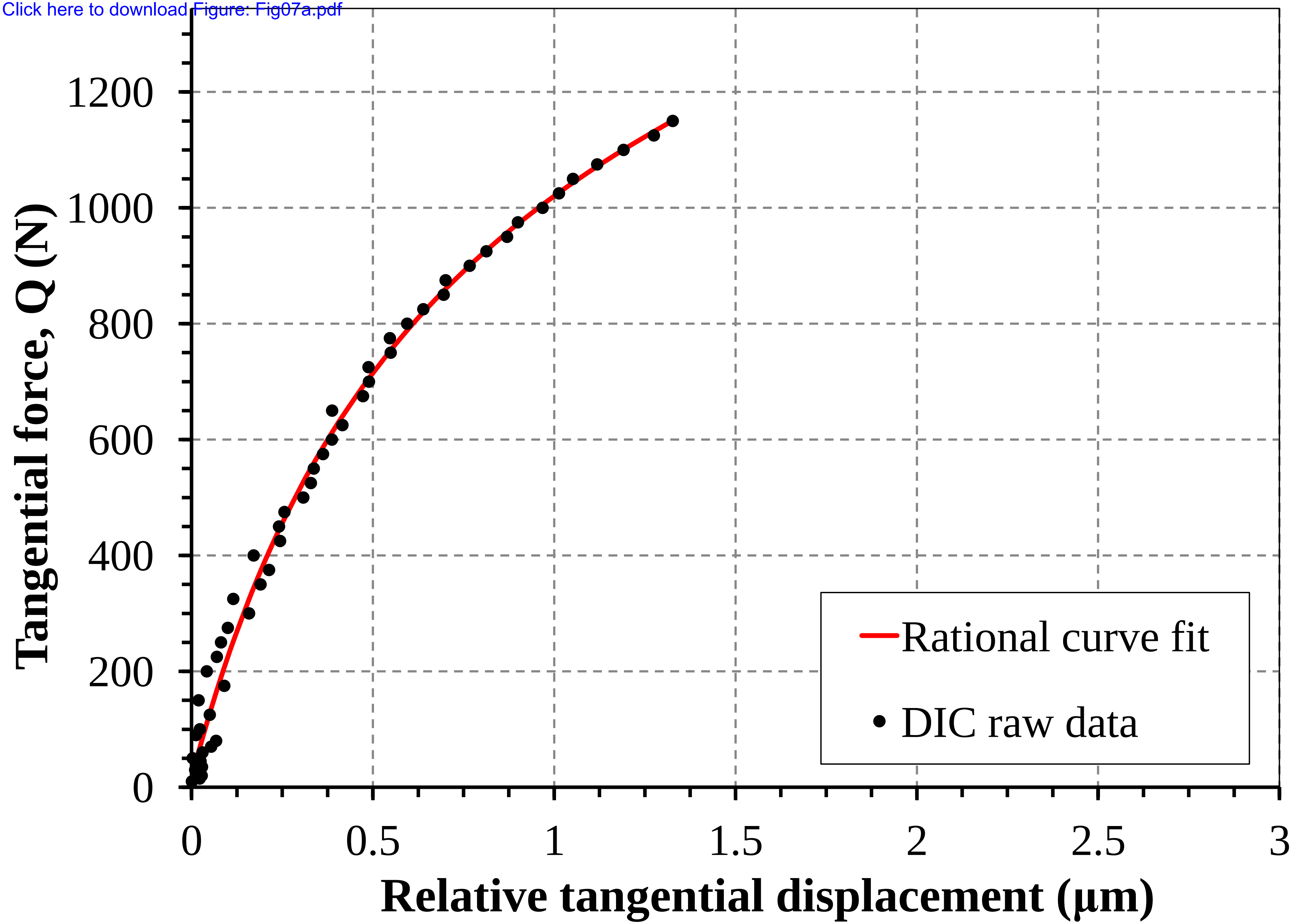

Figure 7b

Click here to download Figure: Fig07b.pdf

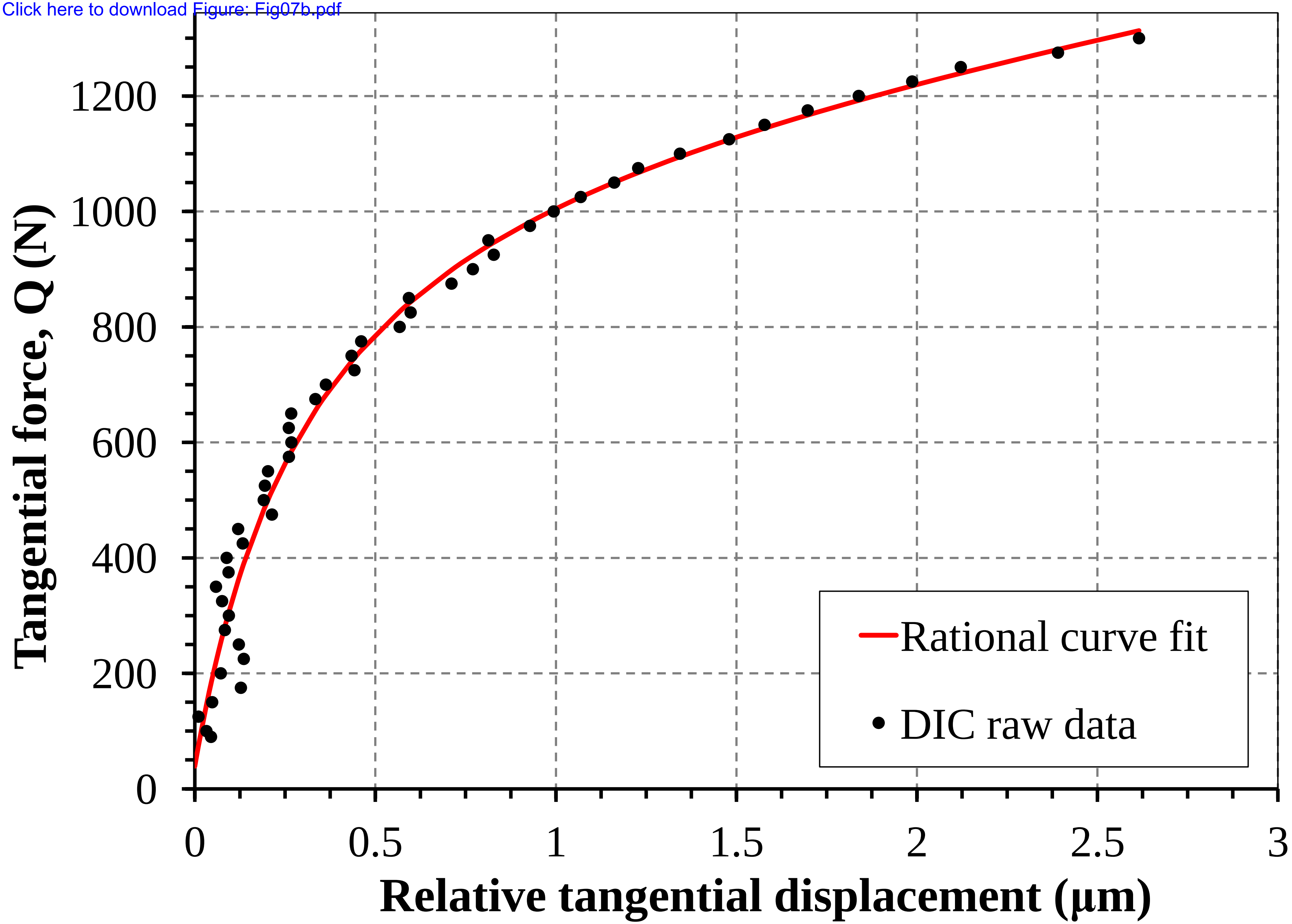

Figure 7c
Click here to download Figure: Fig07c.pdf

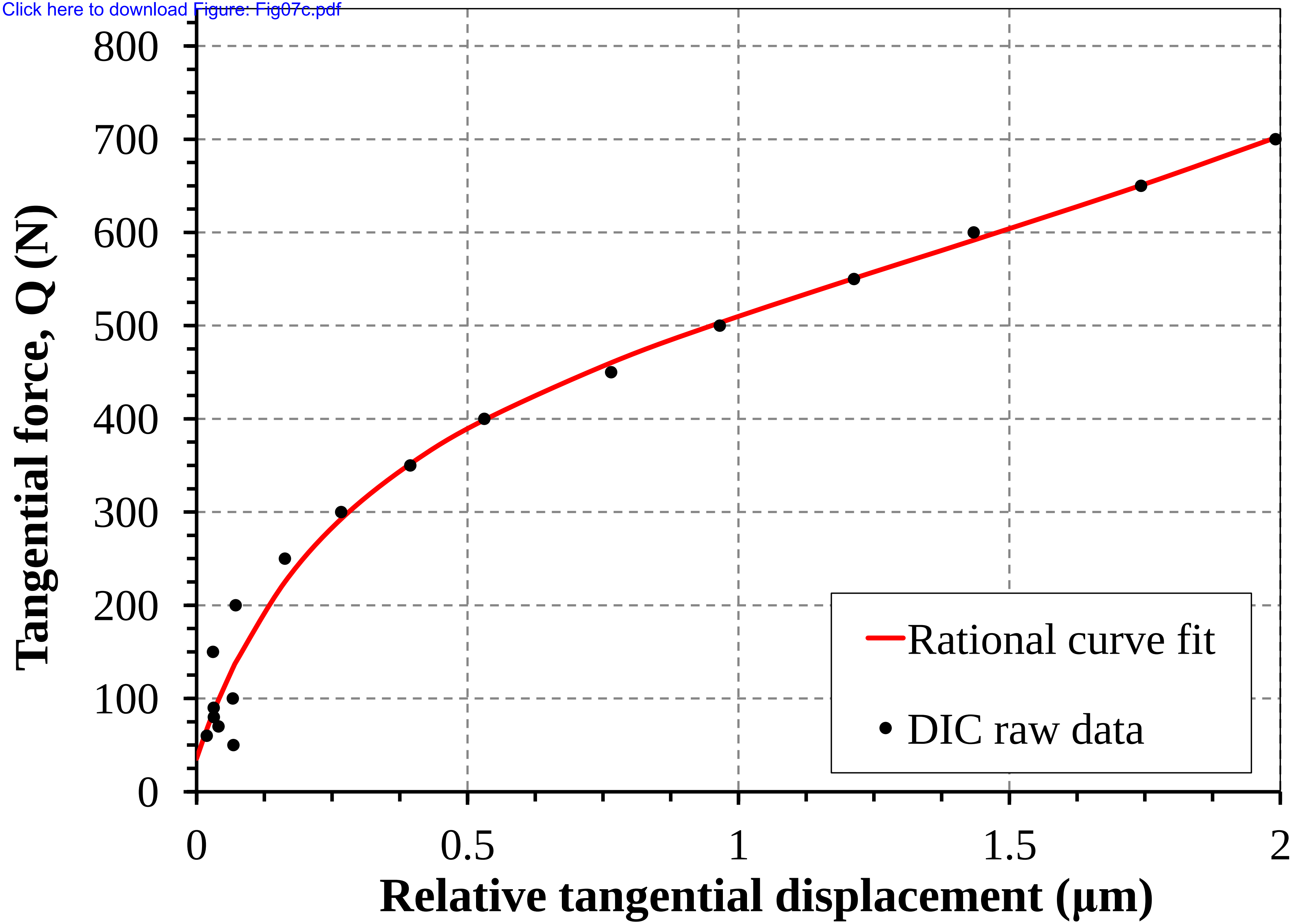

Figure 7d

Click here to download Figure: Fig07d.pdf

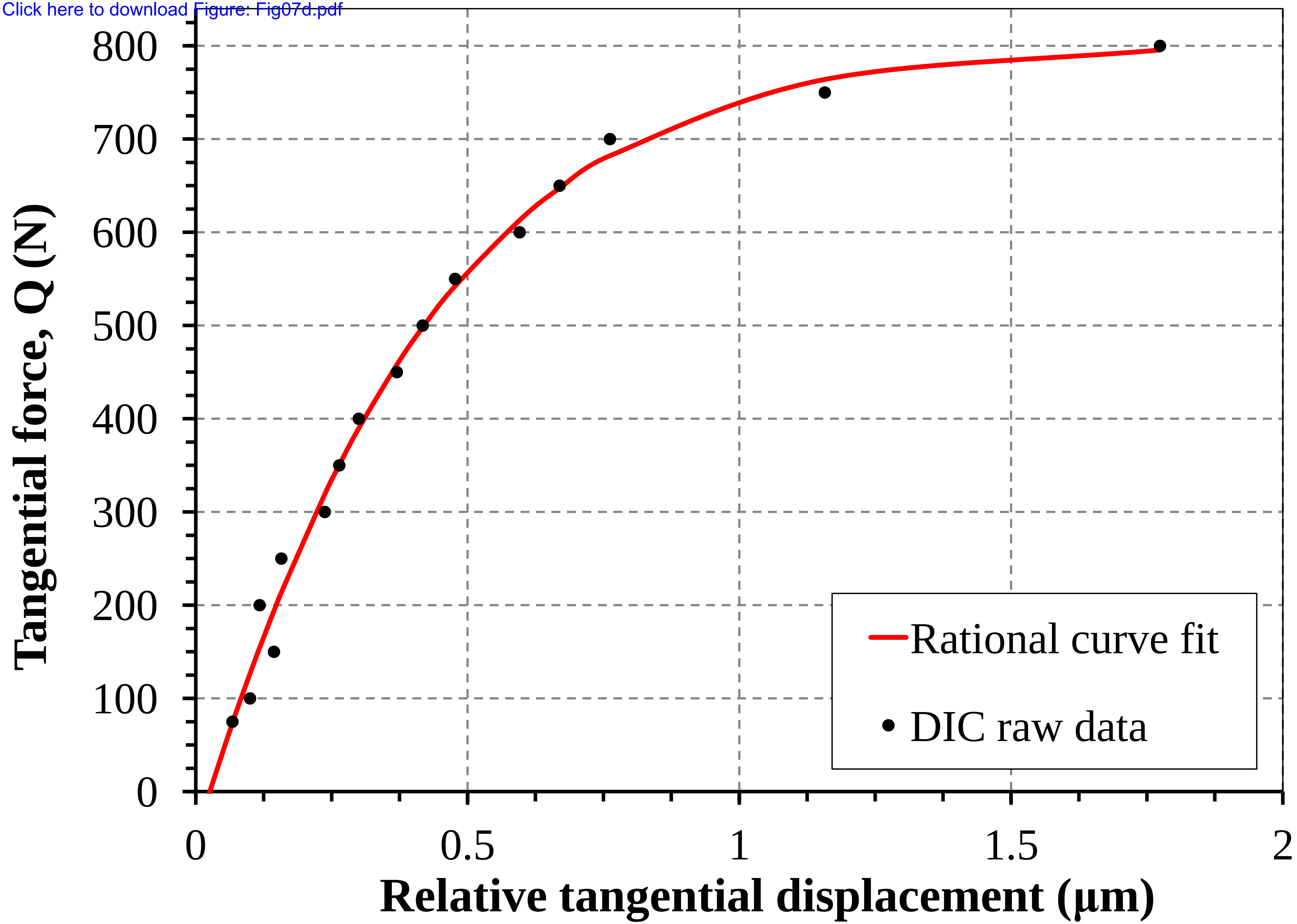

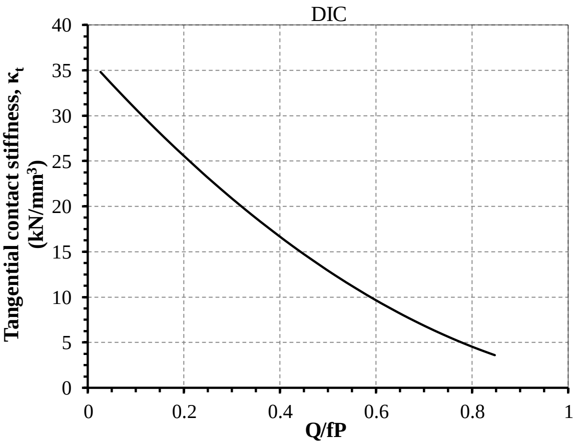
DIC
Tangential contact stiffness, κt (kN/mm3)
Q/fP
0
5
10
15
20
25
30
35
40
0
0.2
0.4
0.6
0.8
1

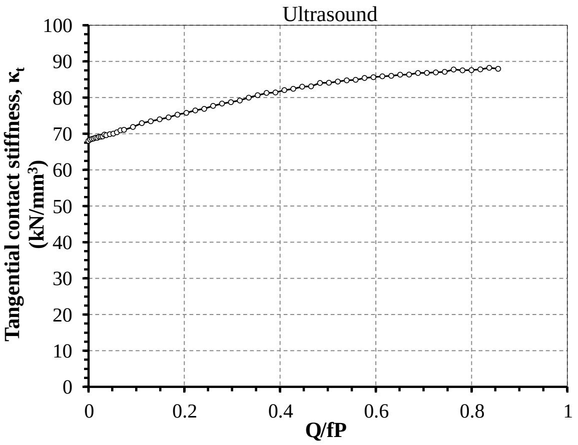
Ultrasound
Tangential contact stiffness, κt (kN/mm3)
Q/fP
0
10
20
30
40
50
60
70
80
90
100
0
0.2
0.4
0.6
0.8
1

8b
Click here to download Figure: Fig08b.pdf

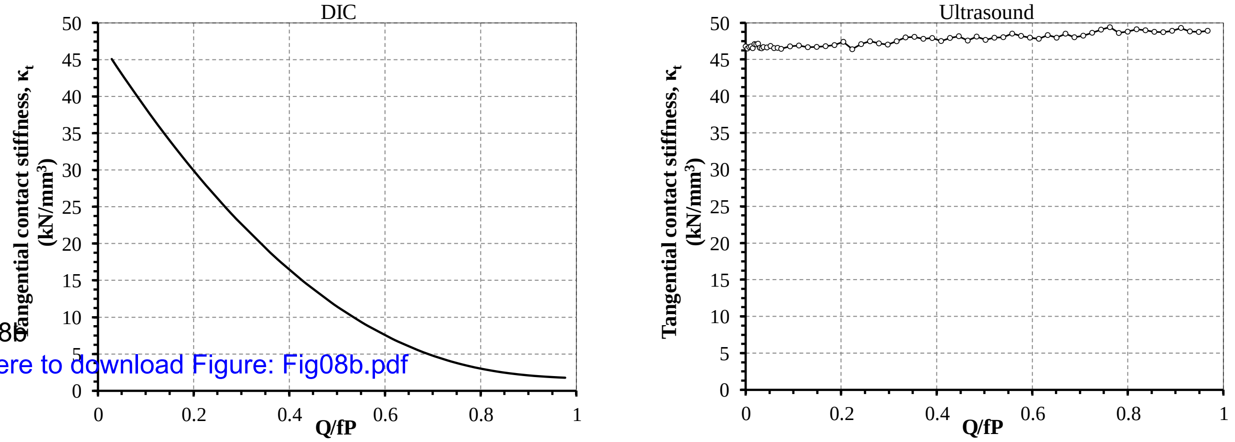

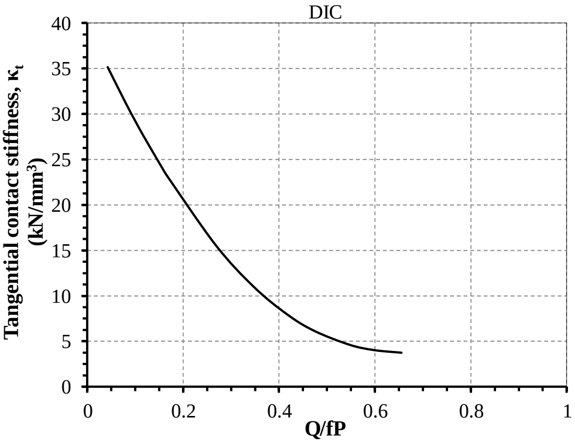

DIC
Tangential contact stiffness, κt (kN/mm3)
Q/fP
40
35
30
25
20
15
10
5
0
0
0.2
0.4
0.6
0.8
1

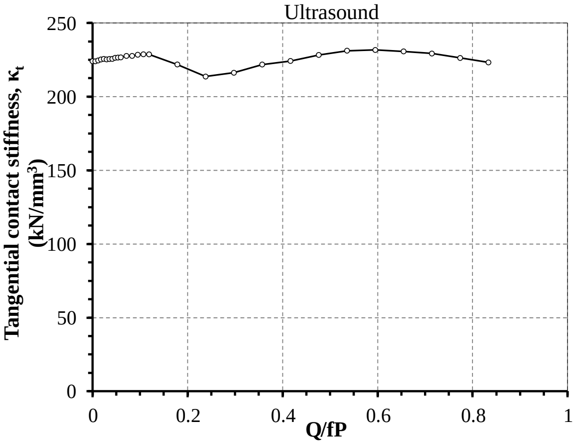

Ultrasound
Tangential contact stiffness, κt (kN/mm3)
Q/fP
250
200
150
100
50
0
0
0.2
0.4
0.6
0.8
1

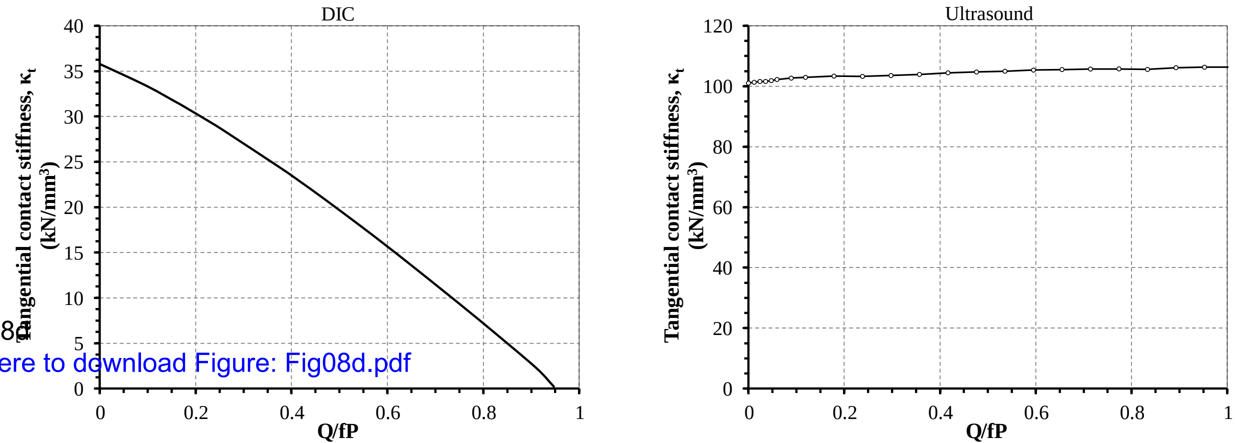
DIC
Tangential contact stiffness, κ_t (kN/mm^3)
40
35
30
25
20
15
10
5
0
0
0.2
0.4
0.6
0.8
1
Q/fP
Ultrasound
Tangential contact stiffness, κ_t (kN/mm^3)
120
100
80
60
40
20
0
0
0.2
0.4
0.6
0.8
1
Q/fP

Figure 9

Click here to download Figure: Fig09.pdf

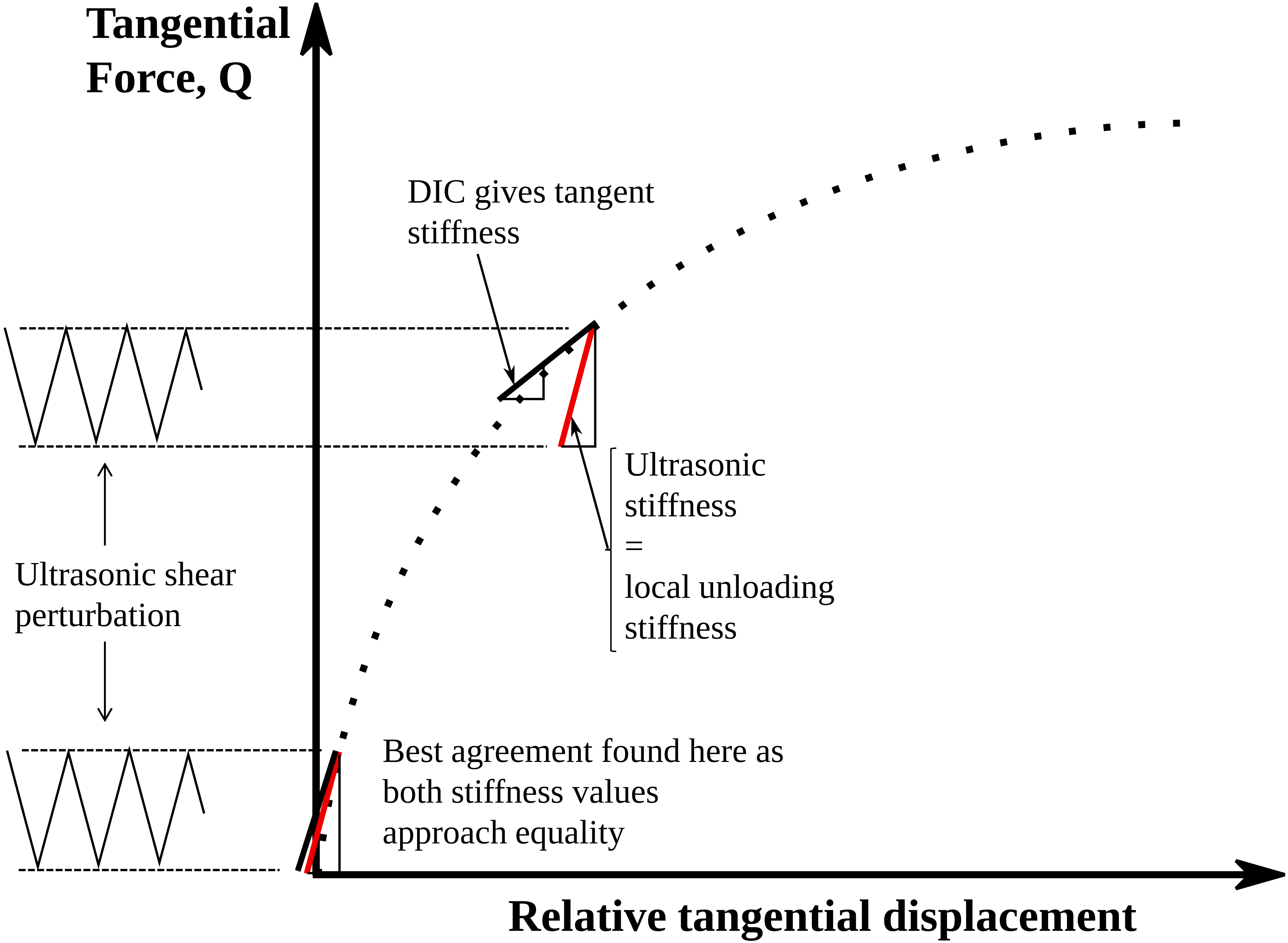

Figure 10

Click here to download Figure: Fig10.pdf

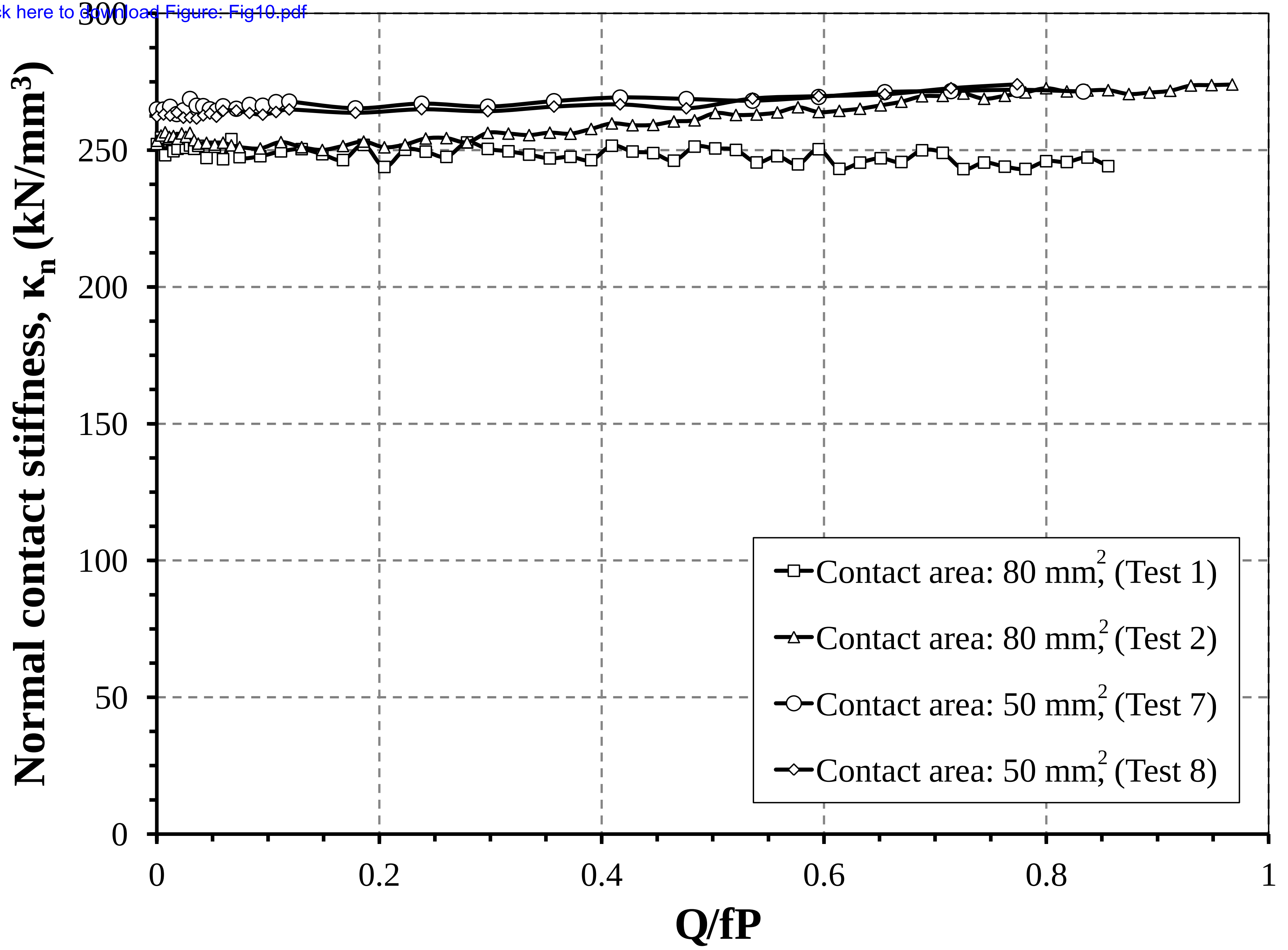

Figure 11a

Click here to download Figure: Fig11a.pdf

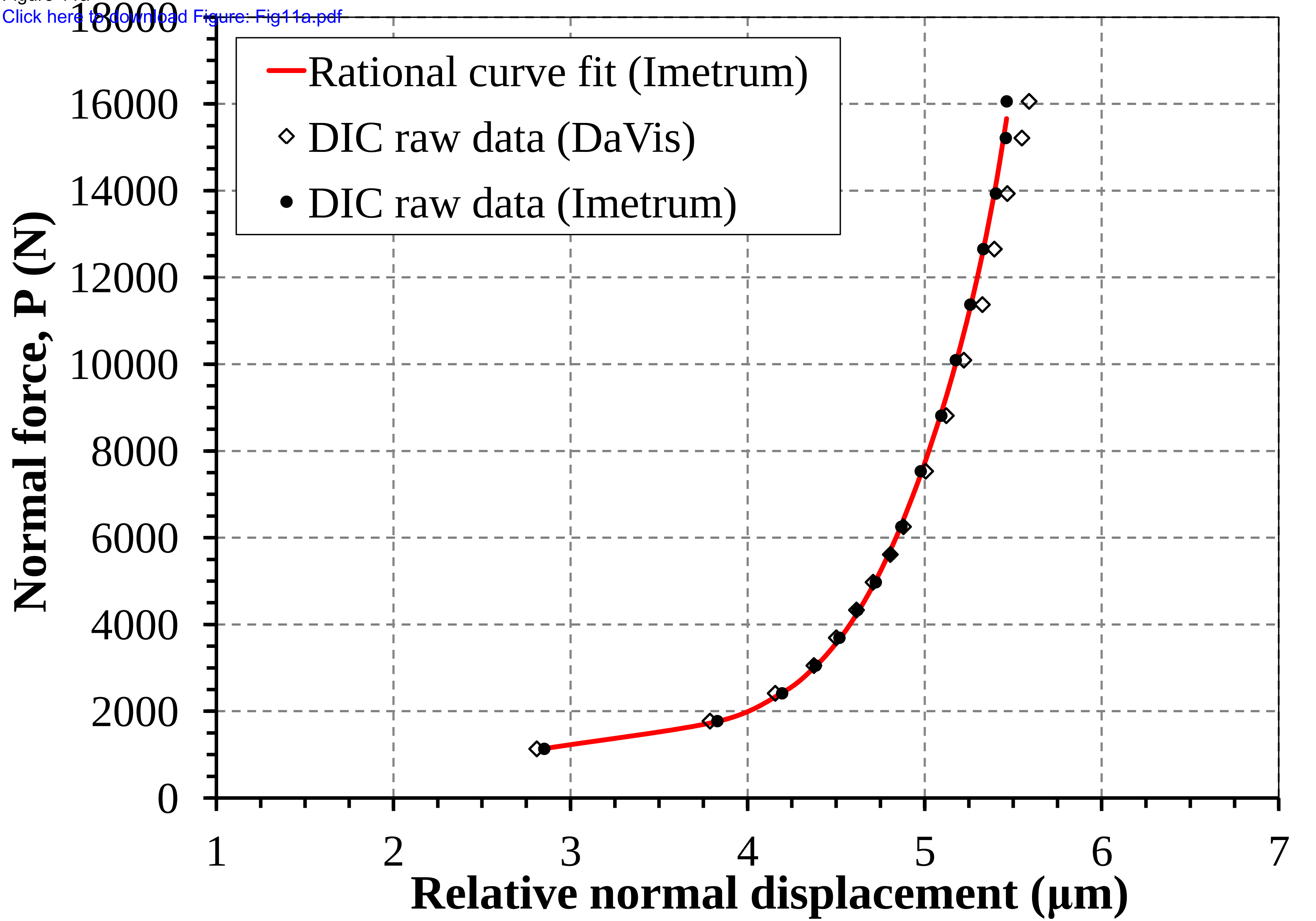

Figure 11b
Click here to download Figure: Fig11b.pdf

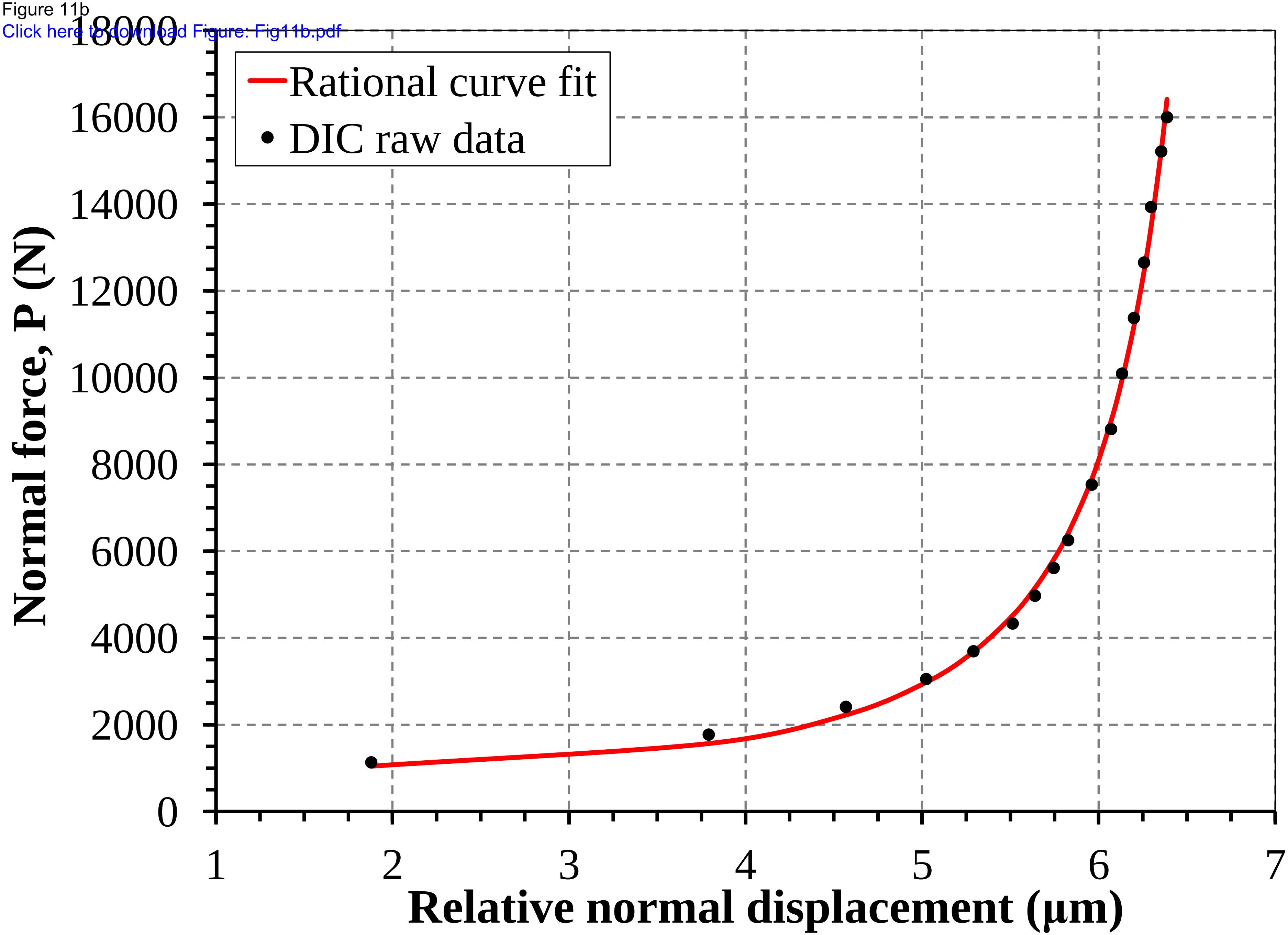

Figure 11c
Click here to download Figure: Fig11c.pdf

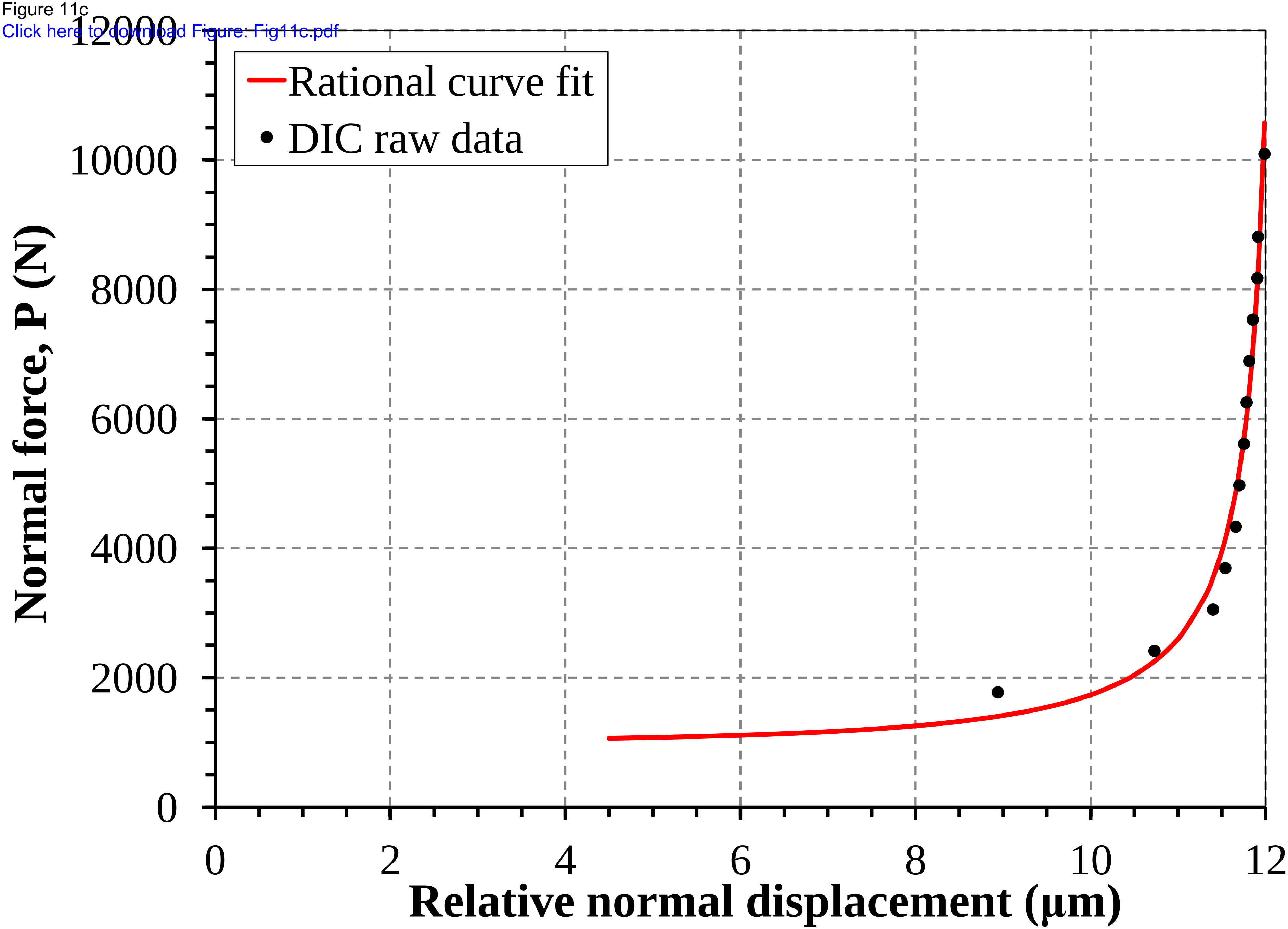

Figure 11d
Click here to download Figure: Fig11d.pdf

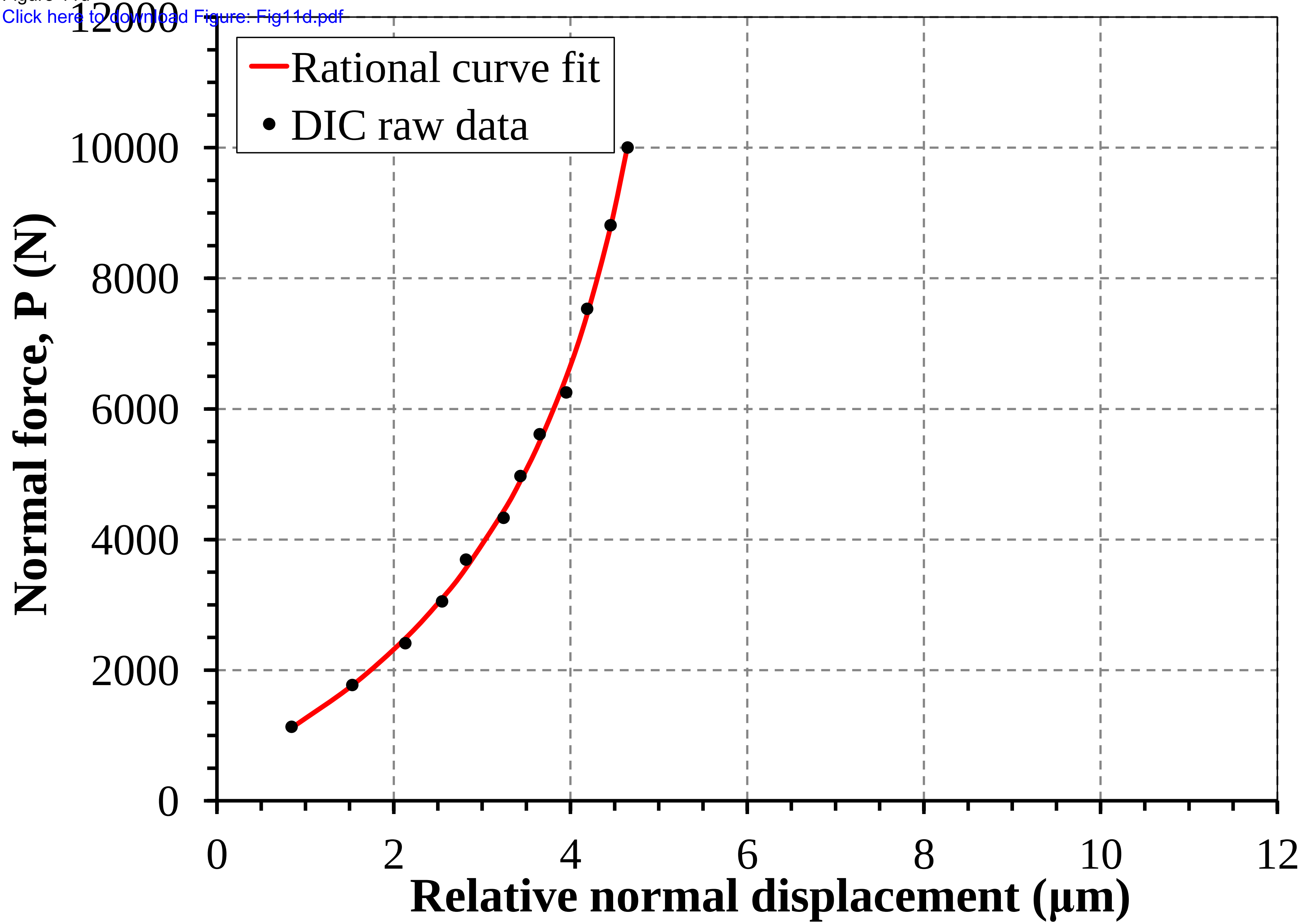

Figure 12a
Click here to download Figure: Fig12a.pdf

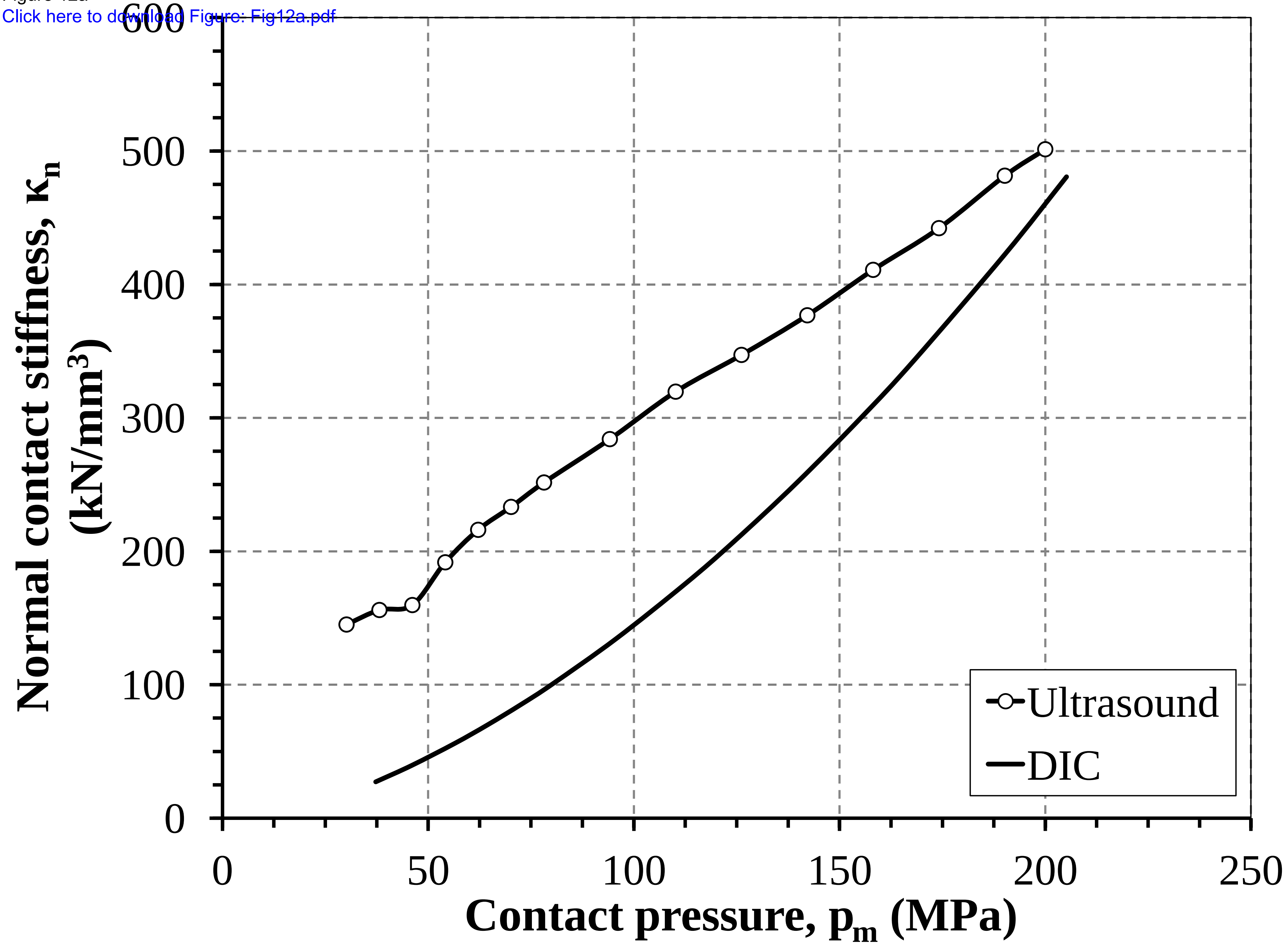

Figure 12b
Click here to download Figure: Fig12b.pdf

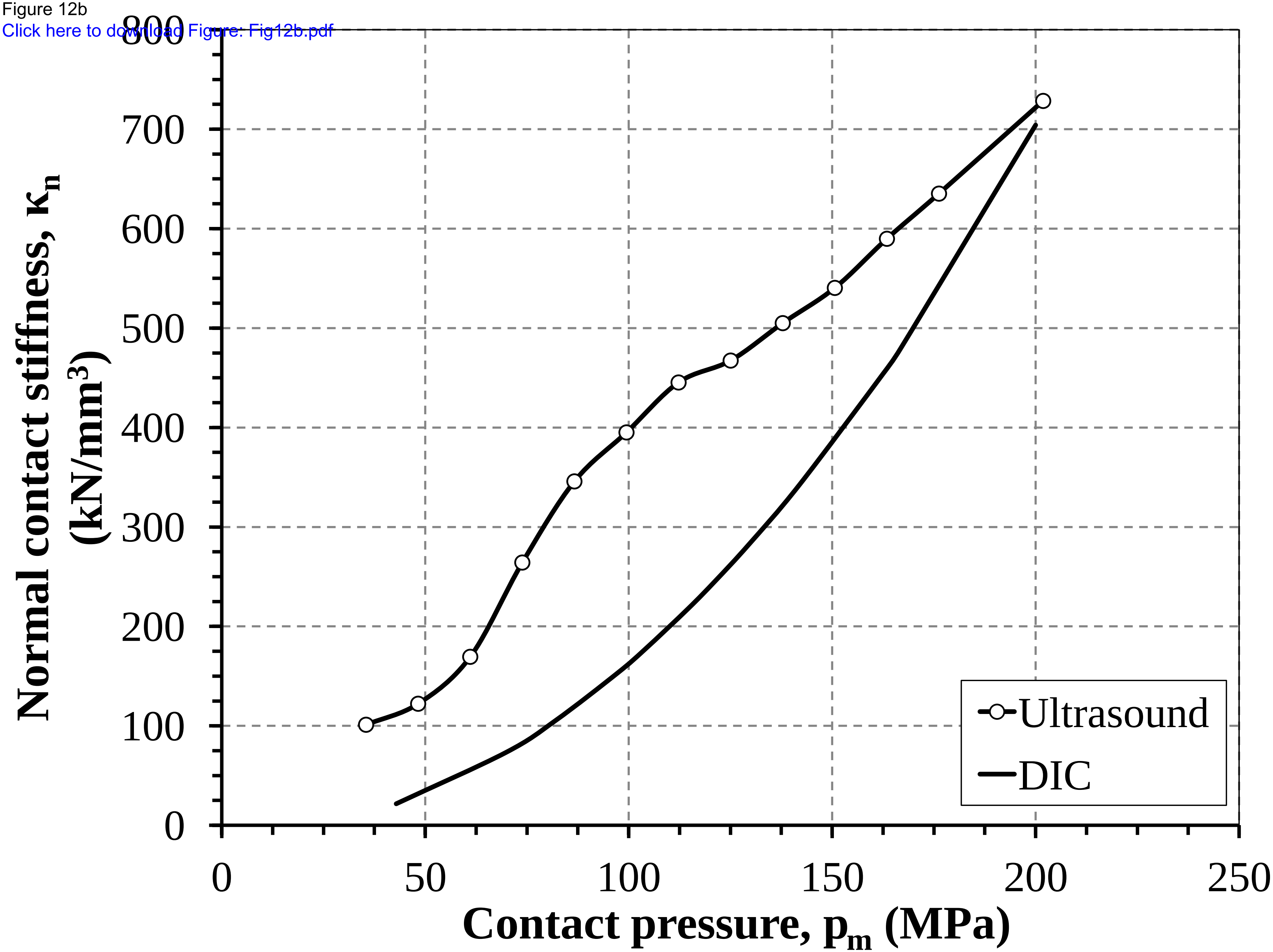

Figure 13
Click here to download Figure: Fig13.pdf

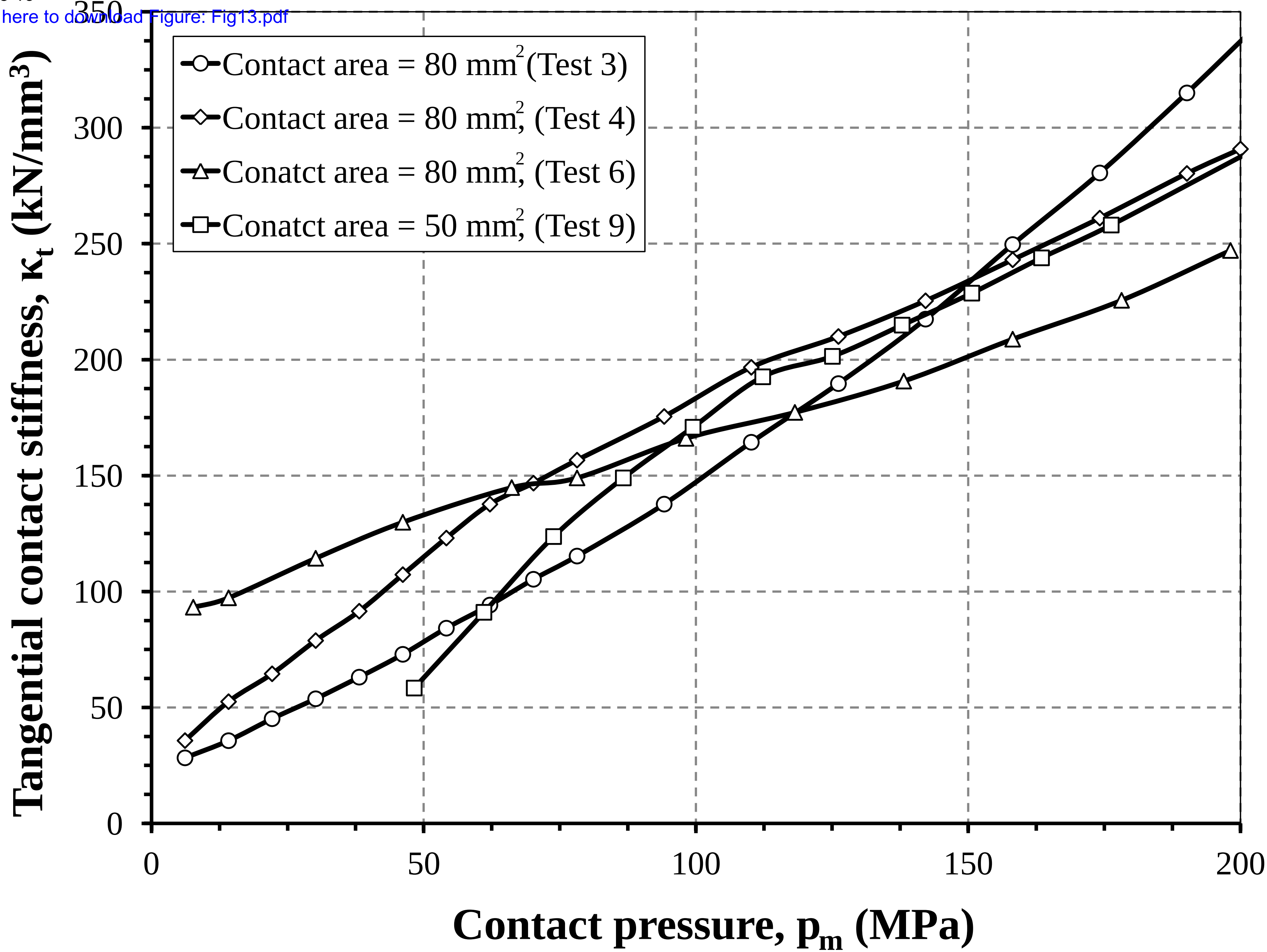

Figure 14a
Click here to download Figure: Fig14a.pdf

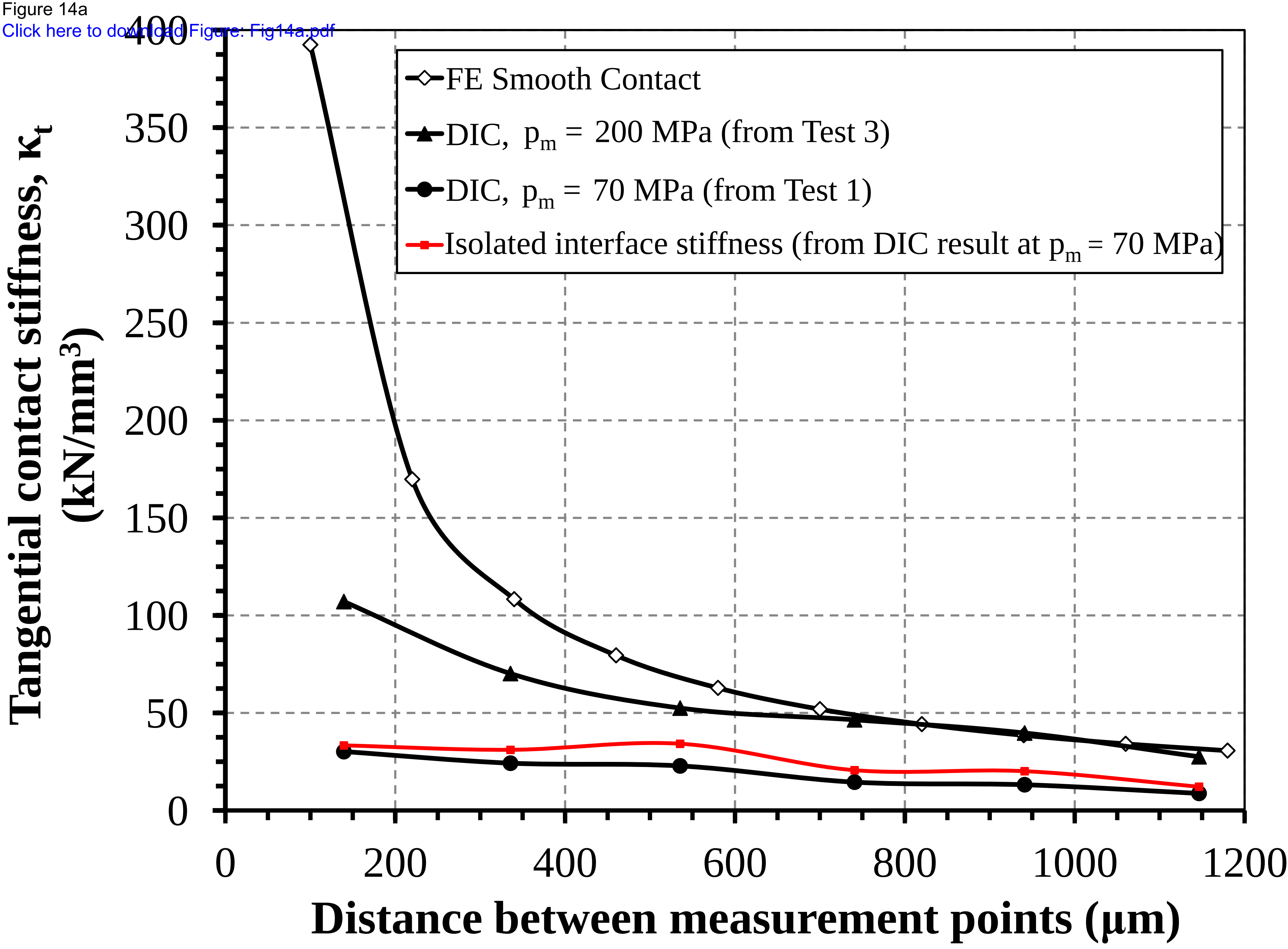

Figure 14b
Click here to download Figure: Fig14b.pdf